Abstract

VAN MAANEN, GUILLERMO JOSE. Morphological and Property Analyses of Multicomponent Block Copolymer Nanocomposites Gels. (Under the direction of Dr. Richard J. Spontak)

Thermoplastic elastomer gels (TPEGs), molecular networks composed of a microphase-separated multiblock copolymer swollen to a large extent by a low-volatility midblock-selective solvent, are ubiquitous in a wide range of contemporary technologies, including home and office products, athletic equipment and telecommunications devices. In this work, we investigate the effect of several network-forming nanoscale modifiers — two different silica nanoparticles, 3 different nanoclays, a multiwalled carbon nanotube and a semicrystalline homopolymer — on the property development of a TPEG prepared from a microphase-ordered poly(styrene-*b*-(ethylene-*co*-butylene)-*b*-styrene) (SEBS) triblock copolymer imbibed with an EB-compatible aliphatic mineral oil. Dynamic rheological measurements of the resultant nanocomposite TPEGs (NCTPEGs) confirm that addition of these modifiers tends to increase the linear viscoelastic threshold, the dynamic elastic modulus (G') and the flow onset temperature (where G' plummets) of the parent TPEG. Variable-temperature stress-relaxation studies indicate that these NCTPEGs undergo substantial relaxation irrespective of added modifier at temperatures above ~60°C. Complementary x-ray diffraction analysis reveals that the nanoclay particles used to generate three series of the NCTPEGs examined here are swollen with copolymer and/or solvent and are therefore intercalated.

MORPHOLOGICAL AND PROPERTY ANALYSES OF MULTICOMPONENT BLOCK COPOLYMER NANOCOMPOSITE GELS

by

GUILLERMO JOSÉ VAN MAANEN

A thesis submitted to the Graduate Faculty of
North Carolina State University
in partial fulfillment of the
requirements for the Degree of
Master of Science

MATERIALS SCIENCE AND ENGINEERING

Raleigh

2004

APPROVED BY:

_____	_____
Dr. Jerome J. Cuomo	Dr. Hans Conrad

_____
Dr. Richard J. Spontak
Chair of Advisory Committee

Padre y Madre… GRACIAS

B , thank you for being by my side!

Biography

Guillermo J. van Maanen was born in Caracas, Venezuela on June 21, 1979 to Willem and Ylayaly van Maanen. He is four years younger than his brother, Alejandro. He attended Colegio Champagnat, catholic school part of the Marist order, from kindergarten up to high school. After graduating from high school, Guillermo decided to enroll in the Materials Science and Engineering department at the Universidad Simon Bolivar due to his intrigue in understanding the properties of materials. After 3 years, his family moved to Boca Raton, Florida due to political problems in the country; Guillermo decided to attend NC State University. While an undergraduate student he met Dr. Rich Spontak and Dr. Phil Russell; he took a position at Analytical Instrumentation Facility and started conducting research with Dr. Spontak. In May 2002, Guillermo received his B.S. in Materials Science and Engineering with honors. Now as a graduate student he continued his work for Dr. Spontak, concentrating on the development of block copolymer nanocomposite gels and on the characterization of these. For the duration of his graduate career Guillermo served as a teaching assistant for introductory classes to Materials Science and Engineering. He will receive his Masters of Science degree in August 2004.

TABLE OF CONTENTS

LIST OF FIGURES

Chapter 1: Introduction

1.1 Theory of Block Copolymers

It has long been recognized that two or more polymers may be blended together to form a variety of biphasic morphologies that potentially offer a desirable combination of the parent characteristics.[1] However it may be difficult or even impossible in practice to achieve such combinations through simple blending strategies because of inherent or fundamental problems associated with crystallinity, degradation and specific intermolecular interactions.[2] Most polymer pairs are thermodynamically immiscible due to a positive enthalpy of mixing (endothermic mixing) and a negligibly low entropy of mixing.[3] Such immiscibility accounts for the generation of a heterogeneous blend, which successfully imparts the properties of the parent polymers to the blend. However, the interface between the coexisting phases may lead to challenges, with high interfacial tension and poor adhesion between the two phases promoting the most common problems.[4] The interfacial tension, along with intrinsically high viscosities, may greatly hinder satisfactory dispersion of the two constituent species and give rise to their subsequent lack of stability. Poor adhesion, for example, leads to the very weak and brittle mechanical behavior often observed in dispersed blends.[5]

Linear block copolymers are bicomponent macromolecules formed when two or more chemically distinct polymer blocks are covalently joined, thereby forming long sequences ("blocks") of repeat units that may be thermodynamically incompatible.[6] If the blocks are sufficiently incompatible, they will spontaneously segregate on the molecular

scale, forming a variety of nanostructures, some of which exhibit long-range order on the order of the gyration radius of the nanostructure-forming block(s).[7] In this regard, block copolymers behave in similar fashion to small-molecule amphiphiles and are commonly referred to as macromolecular surfactants.[8] In contrast to crystalline solids (including those composed of small-molecule amphiphiles), wholly amorphous block copolymers are commonly characterized by liquid-like disorder on the molecular scale and, depending on their incompatibility and composition, a high degree of order at longer length scales. The various nanostructures formed by microphase-ordered block copolymers impart these fascinating materials with useful and desirable properties. A stunning array of molecular architectures, not all of which are linear, can be generated using modern synthetic chemistry techniques[9] and used to develop multifunctional materials with tailored mechanical, optical, electrical and thermal properties. Two parameters are commonly used to classify different molecular architectures:[10] (i) the number of chemically distinct blocks, and (ii) linear versus branched sequencing of the blocks. The simplest and most studied architecture is the AB diblock copolymer, which is a linear macromolecule composed of a sequence of type "A" units covalently bonded to a sequence of type "B" units. Another architecture that has received much attention since its inception as a thermoplastic elastomer[6] is the linear ABA triblock copolymer due to its ability to form a connected molecular network. A recent development extending the utility and interest of triblock copolymers is the synthesis of model ABC triblock copolymers.[11] Block copolymers may alternatively possess a branched architecture, which yields star and miktoarm copolymers. In this study, however, only linear block copolymer molecules are considered further. For a given type of copolymer, another useful design variable is the molecular weight (M) or

overall degree of polymerization ***N***. Since the blocks are independently produced, their degrees of polymerization can be controllably varied, which yields another design parameter, namely, the copolymer composition (f, where f is expressed in terms of one or more of the species present).

1.1.1. Thermodynamics of Block Copolymers and Phase Behavior

As alluded to above, the unique properties of block copolymers rely on their mesoscopic (ca. 10 nm scale) self-assembly in the molten and solution states. Microphase separation generally describe the formation of detectable microphases, whereas microphase ordering considers the possibility that the microphases are sufficiently periodically arranged to exhibit crystallographic symmetry.[10] Microphase separation of block copolymers is generally driven by the chemical incompatibility between the constituent blocks,[11] although compressibility effects may likewise promote microphase separation.[12] Recall that the entropy of mixing of dissimilar macromolecules is relatively small since it varies inversely with molecular weight. Packing considerations associated with the configurational entropy may, however, become non-negligible at nanoscale dimensions.[13] Enthalpic contributions to the free energy reflect chemical and structural differences between the units comprising sequences within the copolymer molecule and are often responsible for demixing. The Flory-Huggins interaction parameter, χ, embodies these contributions by describing the pairwise free energy of contacts between such units.[14] This parameter derives from quasichemical theory of mixtures and relates to the difference in interaction energies: $\chi \alpha \varepsilon_{AB} - (\varepsilon_{AA} + \varepsilon_{BB})/2$, where ε_{ij} (i,j = A or B) denote intermolecular

interactions. Positive values of χ indicate a net repulsion between A and B, whereas a negative χ value provides evidence for negative deviation from Raoultian behavior and a preference to mix. In a polymer blend, the Flory-Huggins theory predicts[14] that phase separation should occur at a thermodynamic incompatibility (expressed as the product of χ and N) equal to 2. While χ is normally close to zero for polymer isotopes such as polystyrene and *d*-polystyrene, Bates et al.[15] have demonstrated that such isotopes become immiscible at sufficiently high-molecular weight.

The temperature dependence of χ is commonly expressed as the inverse of temperature, in which case $\chi = A + B/T + C/T^2$, where A, B and C are empirical constants and T denotes absolute temperature. For a conventional polymer blend or block copolymer that exhibits upper critical solution temperature (UCST) behavior (wherein phase or microphase separation occurs only upon cooling), $C = 0$ and $B > 0$.[16] Although χ is tabulated for numerous polymer blends and may be accurately estimated from solubility parameters (according to $\chi = v\Delta\delta^2/RT$, where v is the average molar volume of the polymers/blocks, $\Delta\delta$ is the difference in solubility parameters and R is the universal gas constant), the covalent linkage of a block copolymer molecule often results in subtle changes to the form of $\chi(T)$. Thus, to predict the phase behavior of a block copolymer, it is best to ascertain $\chi(T)$ directly by small-angle scattering measurements (using x-rays or neutrons) for a given molecule.

In a block copolymer, the chemically dissimilar sequences are tethered together (connected by covalent bonds). Thus, a sufficiently incompatible copolymer molecule cannot phase separate at macroscopic dimensions as the equivalent polymer blend would.

For typical monomer pairs that do not exhibit strong specific interactions (e.g., hydrogen bonding) χ is positive and small compared with unity. To put this in context, χ between polystyrene and polyisoprene is on the order of 0.1 at ambient temperature).[10] The tendency of two blocks to microphase-separate in the case of block copolymers (or to phase separate in the case of two homopolymers) is proportional to the thermodynamic incompatibility χN.[17] According to the seminal mean-field theory of Leibler,[18] a symmetric AB diblock copolymer melt ($f = 0.5$) will remain disordered up to a critical χN value of about 10.5 Recall that for a comparable polymer blend, the critical χN was only 2,[19] which means that, at constant N and assuming the same $\chi(T)$ functionality for the copolymer and blend, the copolymer must be cooled to substantially lower temperature to induce microphase separation relative to the blend.

If it were not for the covalent bond between the contiguous repeat unit sequences, block copolymers would undergo macrophase separation. Unlike in a homopolymer blend, the thermodynamic forces responsible for driving phase separation in a block copolymer melt are counterbalanced by entropic considerations arising from block connectivity. Numerous theoretical studies and computer simulations[20-22] have repeatedly shown how chain elasticity, for instance, plays a role in block copolymer thermodynamics. To ensure that the dissimilar A and B sequences of a microphase-separated copolymer molecule are separated, a copolymer molecule must adopt an extended configuration, rather than its unperturbed random-coil (Gaussian) configuration.[10] As there are fewer configurations available to extended polymer chains relative to their native randomly coiled state, an entropic restoring force limits the size scale of phase separation between the A and B blocks to mesoscopic dimensions.

At values of χN (high temperatures or low molecular weights) below the critical value signifying microphase separation, the copolymer exists in a homogeneous state in which the different blocks are mixed together at the molecular level.[23] At values of χN above the microphase-ordering transition, four characteristic morphologies have been observed to date in neat AB diblock and ABA triblock copolymers: spheres (see Figure1.1)

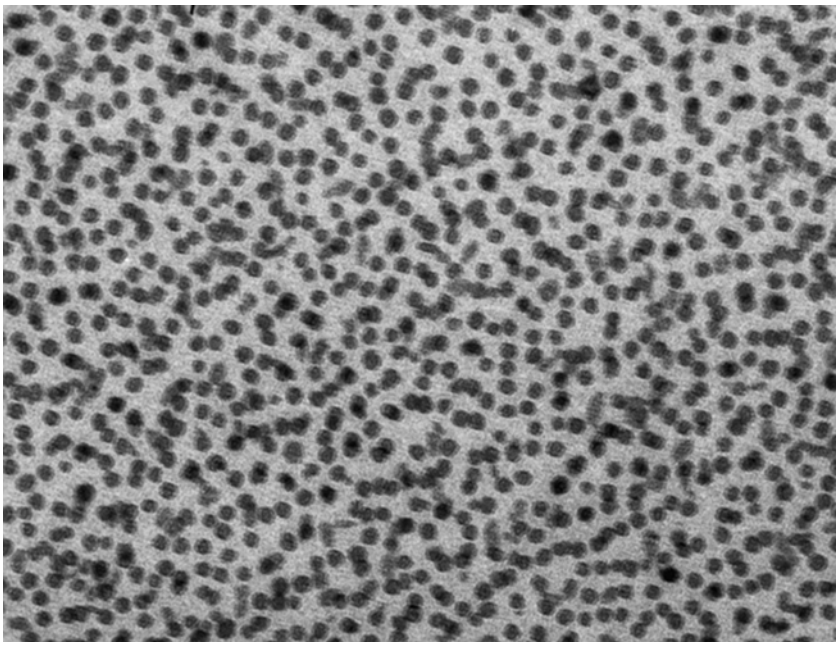

Figure 1.1: TEM image that shows spherical morphology in a SEBS/Mineral oil system

arranged on a body-centered cubic lattice (spheres on a face-centered-cubic lattice have been observed in a solvated block copolymer), hexagonally-packed cylinders, bicontinuous channels (see Figure 1.2)

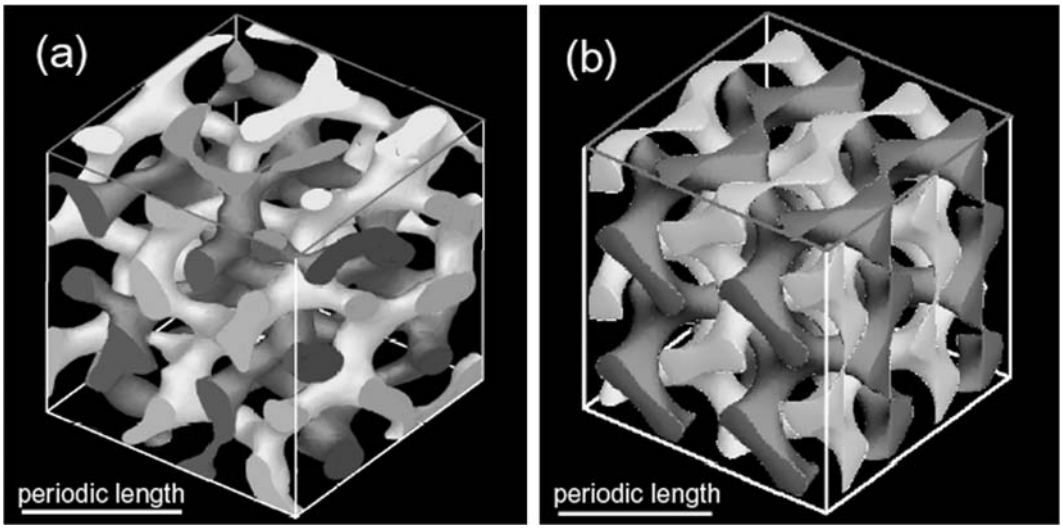

Figure 1.2 - Gyroid morphology

and co-alternating lamellae.[24] In neat copolymers, the microphase-ordered morphology is most strongly affected by the fraction *f*, which is implicitly expressed here in terms of A. If $f \leq 0.18\text{-}0.23$, then spheres of A (spherical micelles) typically form in a matrix of B. If *f* is increased to around 0.30, then cylinders of A (cylindrical micelles) can be expected. As *f* is increased just slightly higher, bicontinuous channels possessing three-fold symmetry (the gyroid) form. For nearly equal volume fractions of A and B, lamellae, also referred to as bilayers or bilayered sheets, develop. If *f* is increased further, the inverse morphologies appear with A comprising the matrix. This set of morphologies corresponds to bicomponent copolymer molecules composed of A and B units. Chemical incorporation of a third unit (to form an ABC triblock copolymer) vastly increases parameter space and the possibility of generating numerous different morphologies (see Figure 1.3).[23]

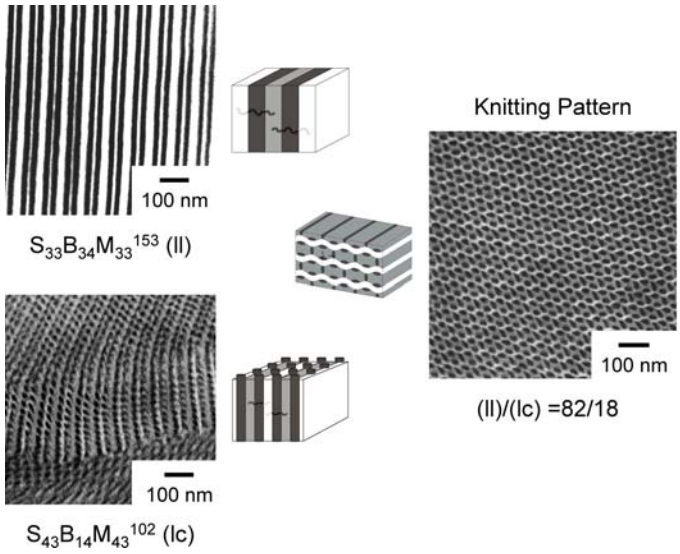

Figure 1.3: Example of morphologies for ABC triblock copolymers

This area of research is beyond the scope of the present study. As mentioned earlier, the microdomains in a microphase-separated AB or ABA block copolymer can be spatially ordered or disordered. Disordered microdomains, usually spheres (micelles), are commonly encountered when the fraction of the microdomain-forming constituent is small (less than ca. 0.10).[25] On the other hand, if the concentration of one of the blocks is greater than ~10% by volume, and the temperature is sufficiently low so that $\chi N > (\chi N)_c$, then the microphases will tend to exhibit long-range order under near-equilibrium conditions (which are not often achieved due to the chain-like nature and high viscosity of the macromolecules). The temperature at which $\chi N = (\chi N)_c$ and the copolymer undergoes ordering from the homogeneous state is generally referred to as the order-disorder transition (ODT).[26] Likewise, a temperature at which a morphological transition occurs

(from one morphology to another within the microphase-ordered envelope) is referred to as an order-order transition (OOT).[27]

An experimental phase diagram for a block copolymer (see Figure 1.4) differs from

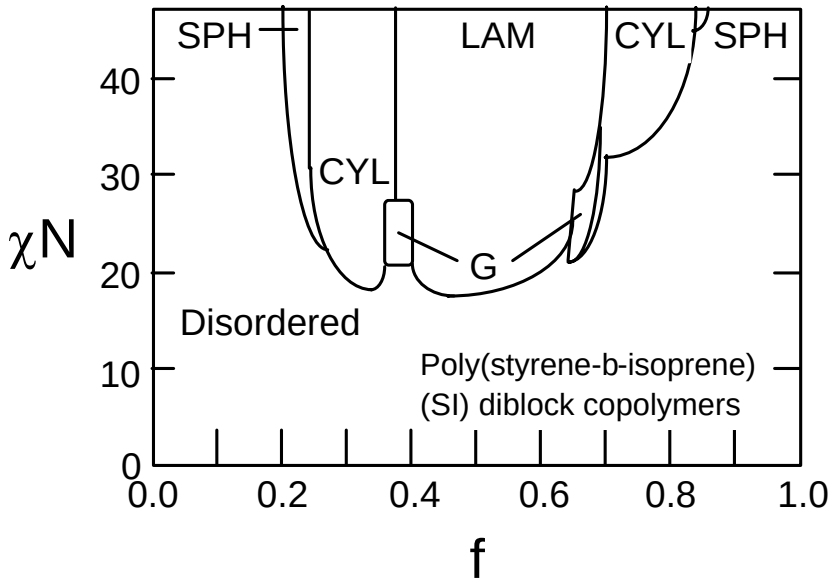

Figure 1.4: Phase diagram for Poly (styrene-b-isoprene) (SI) Diblock copolymer[10]

that of the comparable blend in that each composition requires the laborious synthesis of a new copolymer molecule.[28] Production of a copolymer system with a particular morphology or specific characteristic dimensions can therefore be achieved through tailored synthesis. Alternatively, a microphase-ordered block copolymer can be modified through the addition of a block-specific or parent homopolymer, or a low-molar-mass solvent to form a miscible copolymer/homopolymer blend.[29] Numerous theoretical treatments[23] have been developed to predict the location of the homopolymer within the microphase-ordered morphology and generally contend that the two main considerations in such blends are (i) the homopolymer fraction and (ii) the homopolymer molecular weight

ratio (relative to the host block of the copolymer).[23] It immediately follows that addition of solvent corresponds to the limit of a homopolymer as N goes to unity. The two advantages of adding a block-selective solvent at low concentrations to a microphase-ordered copolymer are that (i) the solvent molecules are completely solubilized within the copolymer matrix and (ii) they are uniformly distributed (not localized) within their host block and consequently wet the resident blocks more effectively than a similarly compatible homopolymer.[30] In both cases (homopolymer and solvent), the additive not only reduces the effective value of χN,[30] but also influences the interfacial curvature of the resultant morphology. Since the phase behavior of symmetric ABA triblock copolymers is qualitatively similar to that of AB diblock copolymers (with reported[31] differences in the value of χN at the ODT and compositions corresponding to OOTs), the strategy described above can be readily applied to microphase-ordered triblock copolymers to produce highly elastic molecular networks.

1.2 Triblock Copolymer Gels

In the present study, a linear poly(styrene-*b*-(ethylene-*co*-butylene)-*b*-styrene) (SEBS) triblock copolymer, an established[32] thermoplastic elastomer (TPE), is used in conjunction with a midblock-selective solvent to form a thermoplastic elastomeric gel (TPEG). This example of a thermally reversible (i.e., physical[33]) gel combines softness and elasticity over a wide temperature range. The midblock-selective solvent employed here is an aliphatic oil that has a low solubility in polystyrene. While previous studies[34] have examined the phase behavior and properties of concentrated SEBS/oil solutions, this study

examines solutions wherein the oil constitutes the major component (90 wt%) and, thus, the matrix. The copolymer self-organizes into discrete, but disordered, S micelles under these conditions. Unlike equivalent diblock copolymers, the EB midblock of each copolymer molecule can form either a loop (the endblocks of the molecule reside in the same S micelle) or a bridge (the endblocks of the molecule reside in different S micelles).[35] By virtue of bridged midblocks or interlaced looped midblocks, neighboring micelles become connected and, at sufficiently high concentration, form a network that is capable of behaving as an elastic solid (i.e., a gel). If looped midblocks contribute to the gel mechanical properties (described below), the micelles are described as "flower-like" and entanglements among adjacent loops are non-negligible.[36] At copolymer (or oil) concentrations where bridged midblocks regulate mechanical properties, the network behaves equivalently as beads connected by elastic springs in the Rouse limit.[36]

Previous rheological studies[37-40] of SEBS/oil TPEGs behave as elastic gels at ambient temperature. Above the glass transition temperature (T_g) of PS, there is an eventual change from a load-bearing gel to a viscoelastic liquid at a copolymer-dependent lattice-disordering temperature.[41] Increasing the temperature beyond this temperature results in the formation of a liquid in which the S blocks become mobile and do not serve as physical crosslinks. One of the main problems encountered in TPEGs containing the SEBS copolymer, or any styrenic copolymer for that matter, is that these transition temperatures are too low for many applications. This shortcoming explains why so much emphasis has been paid to either chemical modification of one of the blocks or physical modification of one of the micelles through incorporation of additives.[41-42] The latter method has proven very effective since properties can be dramatically enhanced with

minimal increase in density due to the low inorganic loading required. Jackson et al.,[43] for instance, have used dynamic rheological methods to show how, by adding the S-selective homopolymer poly(2,6-dimethyl-phenylene oxide) (PPO) to a SEBS/oil gel, the disordering temperature can be increased significantly.

1.3 Formation of Nanocomposites

An intriguing alternative to physical modification of an existing polymer-based gel is to incorporate nanoscale inorganic objects into the gel. By their very nature, such "nanofillers" will possess high-modulus properties that could be imparted to the gel without disrupting the copolymer network needed to retain physical gel characteristics. In fact, at sufficiently high concentrations, such nanofillers may likewise form an ancillary network,[42] leading to hierarchical network structures with synergistic thermo-mechanical properties. In this work, we have examined the strengthening efficacy of a broad series of such nanofillers: three types of organically-modified nanoclays (C30B with hydroxyl termination, C93A with alkyl termination and B38), two types of silica (colloidal silica with native hydroxyl termination and fumed silica with alkyl termination) and a multiwall carbon nanotube. For comparative purposes, an S-compatible semicrystalline homopolymer was likewise dispersed within the copolymer gel network.

Design of a reinforced polymer system with enhanced mechanical, physical and thermal properties requires consideration of the nature and strength of the polymer-filler and filler-filler interactions, as well as the extent of dispersion of the filler.[43-44] While these issues have been known since the early days of polymer composites, they have become

increasingly important in regard to polymer nanocomposites, which contain any nanofiller such that at least one dimension of the filler is on the nanoscale. Several different types of nanocomposites prepared with added particles, fibrils/tubes and layered plates[42-44] have been reported. A profound challenge in the production of these hybrid materials is the dispersion of the nanofiller, which effectively controls the area of interaction between the inorganic species and the organic matrix. One growing class of polymer nanocomposites has been developed through the use of anisotropic organically-modified layered silicates (see Figure 1.5).[43-44]

Figure 1.5: TEM image of a hectorite nanocomposite[44]

On the basis of the strength of the polymer-silicate interaction, three levels of dispersion can be achieved, thereby rendering different materials:[45] **microcomposites** (no polymer is imbibed within the silicate particles), **intercalated nanocomposites** (the interlayer region separating adjacent plates is swollen with polymer) and **exfoliated nanocomposites** (the individual plates of the silicate are uniformly dispersed throughout the polymer matrix). While exfoliated systems are preferable, they are often difficult to

generate due to geometrical restrictions and chemical interactions (polymer-filler or filler-filler).[45] Improved properties have also been reported for intercalated systems. Addition of an organoclay to poly(dimethyl-co-diphenylsiloxane) to form an intercalated nanocomposite, for instance, results in non-Newtonian viscosity at all loadings and a low-frequency elastic modulus plateau.[46] In contrast, an exfoliated nanocomposite derived from poly(dimethylsiloxane) has been reported[46] to exhibit substantial increases in the elastic modulus and viscosity, with minor changes in viscoelastic properties, as the loading was increased. By promoting chemical interactions between the polymer and the organic functionalities on the organoclay, exfoliated nanocomposites based on nylon 6 display a marked difference in viscoelastic properties: the elastic and viscous moduli exhibit a change from liquid-like to pseudo solid-like behavior at low frequencies with as little as 3% silicate.[47] Relevant theories[42] attribute this behavior to the orientation of the plates upon exposure to large-amplitude oscillatory shear.

Most studies of polymer nanocomposites utilize a homopolymer matrix to which a nanofiller is added. Such materials can give rise to unique and totally unexpected property development, such as reverse selectivity in high free-volume polymers[48] or ionic transport in organic batteries.[44] A growing number of studies seeks to elucidate the effect of a physically added nanofiller on the phase behavior and properties of nanostructured polymers, such as microphase-ordered block copolymers.[38] Silva et al.,[45] for instance, have examined the rheological properties of intercalated nanocomposites based on a poly(styrene-*b*-isoprene) (SI) diblock copolymer and a dimethyl/dioctadecyl-substituted montmorillonite (silicate). In this case, they attribute the linear oscillatory shear and stress relaxation behavior to the formation of a percolated silicate network at silicate

concentrations in excess of ~5%. They have also verified that the rheological properties are essentially unaffected by the choice of the chemical nature of the polymer matrix (block copolymer *versus* homopolymer), but are affected by plate dispersion.

Common nanoparticles used as reinforcing agents in polymers are nanostructured carbons (fullerenes and nanotubes) and silicas (fumed and colloidal). The existence of long-range order in these materials is limited to the atomic level and is expected to have little, if any, influence on nonpolar polymer matrices. While nanoparticles may form aggregates that can be described as fractal quantities in polymer matrices,[48] it remains unestablished as to how such quantitation can be used to correlate property development in nanocomposites. In the case of layered silicates, however, the individual plates measure on the order of several nanometers in thickness (comparable in size scale as individual polymer chains) and up to several micrometers in each lateral dimension. Since as-received silicate powder particles consist of numerous stacked layers, analysis of plate separation by x-ray (powder) diffraction can provide valuable information regarding the repeat distance perpendicular to the plates and, hence, the extent of intercalation or exfoliation. In an **immiscible** mixture of polymer and organoclay, the (001) basal reflection does not change in intensity or position. In **intercalated** systems, interlayer swelling results in a shifted basal reflection that corresponds to the larger repeat distance (also termed gallery height). If intercalation is accompanied by unequal swelling, peak broadening and intensity loss will be observed due to a reduction in the degree of coherent layer stacking. When **exfoliation** occurs, the basal reflection disappears completely.[49]

The theoretical framework developed by Giannelis and Vaia,[50] in conjunction with available experimental data,[42,50] suggests that the S blocks, not the I blocks, of a

microphase-ordered SI diblock copolymer is responsible for the intercalation of the dimethyl/dioctadecyl-substituted montmorillonite investigated by Silva et al.[45] According to their prediction, the phenyl groups of S chains experience strong interactions (Lewis base character) with the surface of the silicates. Another feature previously noticed[45] is that the extent of intercalation is independent of the silicate loading. Increased gallery height could be attributed to the incorporation of the unfavorable I block into the interlayer as the S block interacts with the silicate surface. Due to the high bending modulus of the ceramic plates and the high van der Waals forces between the layers, it is virtually impossible for the S block alone to infiltrate the edges and expand the galleries. The presently accepted[42,50] picture of this complex system is that both blocks enter the interlayers and the S block locates close to the silicate surface while the I block occupies the central portion of the interlayer.

Lee et al.[51] point out that the primary factor governing gallery height is the chemistry of the surfactant applied to the surface of the layered silicate. Their conclusion relies on the fact that silicates possess a large surface area (~700-800 m^2/g in the case of montmorillonite) and a moderate negative surface charge, which translates into a cation exchange capacity. Organoclays are expressly modified to improve their exfoliation tendency. In the specific case of cloisite clays, the hydrated metal cation can be replaced with organic cations (such as alkylammonium chloride), thereby imparting a hydrophobic character to the layered silicate and a tendency to exhibit a relatively large interlayer spacing.[51] The cationic head group of the alkylammonium chloride molecule resides at the surface of the layered silicate while the oligomeric tallow species, which could contain polar groups, extend into the galleries. To test their hypothesis, Lee et al.[51] have

investigated the behavior of three random copolymers — poly(ethylene-*r*-vinyl acetate) (**EVA**), poly(ethylene-*r*-vinyl alcohol) (**EVOH**) and poly(ethylene-*r*-vinyl acetate-*r*-vinyl alcohol) (**EVAOH**) — in the presence of two commercially available organoclays treated with different surfactants, one with hydroxyl groups (Cloisite 30B) and the other with alkyl groups (Cloisite 15A). The most enhanced rheological properties are observed in the EVAOH/Cloisite 30B and EVA/Cloisite 15A systems due to enhanced compatibility between the polymer matrix and organoclay. Hoffmann et al.[52] have conducted a similar study using polystyrene homopolymer (PS) and two synthetic micas modified with amine-terminated polystyrene (AT-PS8) or 2-phenylethyamine (PEA). Their results are sensitive to the modified mica employed. Nanocomposites composed of PS100 and the AT-PS8 mica exhibit pseudo solid-like behavior at low frequencies, indicating the formation of a network.

This pseudo solid-like behavior at low frequencies is an interesting feature of silicate-based polymer nanocomposites and warrants additional discussion. Physical displacement (jamming) of dispersed layered silicates due to their highly anisotropic plates and geometric constraints can help to explain the variation in behavior of different intercalated systems at low frequencies.[42] Such behavior is also observed[45] in exfoliated nanocomposites and is explained in similar fashion. These systems might exhibit local correlations despite exfoliation of the plates, thereby forming discrete domains that could impart pseudo solid-like behavior. Beyond a critical loading of layered silicates in an exfoliated system, the layers become incapable of freely rotating/tumbling when subjected to an oscillating shear and it is difficult for the system to relax fully.[45]

1.4 Silica and Triblock Copolymer Gels

In the present study, two different types of silica nanoparticles have been added to the SEBS/oil TPEGs for reinforcement purposes: **colloidal silica** (particle size of 20 nm, hydroxyl termination) and **fumed silica** (particle size of 12 nm, alkyl termination). In contrast to the layered silicates, the silica nanoparticles are anticipated to form flocs at low concentrations and a secondary elastic network at high concentrations (see Figure 1.6).[53]

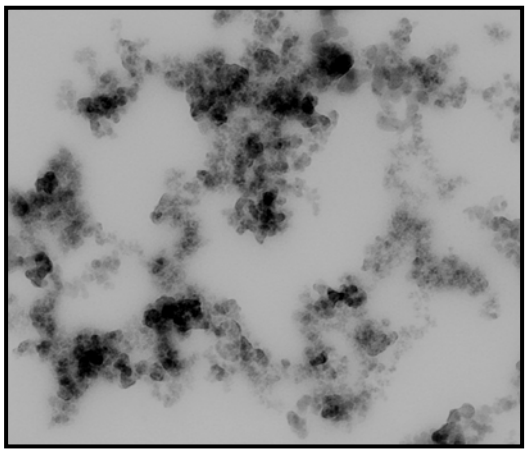

Figure 1.6: TEM image of fumed silica in poly(ethylene glycol). Noticed the development of a network by the fumed silica.[47]

The surface chemistry will greatly influence the ability of the nanoparticles to be uniformly dispersed throughout the gel medium. While SEBS/oil TPEGs are commercially used in a wide variety of products ranging from athletic shoes to shock absorbing media, only one other study to date has attempted to reinforce the matrix by adding silica nanoparticles.

Theunissen et al.[54] have investigated concentrated TPEGs (18.5% SEBS copolymer) and different types of silica (hydroxyl versus alkyl surface groups) at a constant silica loading of 2.2%. Using both small-angle neutron scattering (SANS) and small-angle x-ray scattering (SAXS), they have sought to elucidate the effect of the added silica on the existing polymer nanostructure. The SAXS analysis of the unmodified block copolymer gel reveals the structure factor and form factor. The structure factor contains information regarding the size and shape of the S micelles, and the associated peaks are a consequence of *intra*microdomain interference.[54] The form factor provides information on the arrangement of the S micelles within the oil-rich matrix and arises due to *inter*microdomain interference.[54] Comparable analysis of the silica-modified gels yields no useful information (except an increase in scattering intensity at low scattering vectors, which is attributed to large aggregates of silica particles) about the system. Thus, scattering from the silica nanoparticles interferes with scattering from the copolymer micelles. Complementary SANS analysis shows a broad, but distinct, peak confirming the existence of the intrinsic micellar network. The broadened peak is attributed to the heterogeneous distribution of S micelles. Most of the silica nanoparticles used are incompatible with S, as evidenced by a position-invariant form factor of the S micelles. Moreover, addition of silica necessarily requires a reduction in solvent content, resulting in an effective reduction in intermicellar distance.

Theunissen et al.[54] have also examined their silica-reinforced TPEGs by simultaneous dynamic rheology, which is a characterization technique that is well-suited for the investigation of nanostructured gels. Within the linear viscoelastic regime, the material properties (e.g., the elastic and viscous moduli) are independent of strain

amplitude, thereby permitting quantitative comparison of different materials.[54] Rheology can be used to ascertain the molecular contributions responsible for the measured moduli (as in the case of flowered micelles[36]), as well as identify salient thermal transitions (such as the ODT or an OOT) and characteristic time scales (such as relaxation times). In the case of the silica-reinforced TPEGs examined by Theunissen et al.,[54] addition of hydrophilic silica promotes increases in both the ODT and the elastic modulus of the gel at ambient temperature. These effects can be enhanced by increasing the hydrophobicity of the nanoparticle surface and making the nanoparticles more chemically compatible with the matrix. Increased compatibility ensures a more homogeneous distribution of nanoparticles within the gel and improved stress transfer between the phases.

This thesis addresses the effects of nanofiller shape, surface chemistry and concentration on the properties of a SEBS/oil TPEG of constant composition (90 wt% oil). It is divided into four additional chapters:

Chapter 2 provides a brief overview of the experimental methods employed.

Chapter 3 compares nanofillers with an organic additive.

Chapter 4 compares the properties of different nanofillers.

Chapter 5 provides general conclusions and recommendations for future work.

1.5 References

1. F.S. Bates; G.D. Wignall. *Macromolecules* 19, 932 (1986).
2. A.J. Ryan. *Nature*, Vol. 1, 8 (September 2002).

3. I.W. Hamley. The physics of block copolymers, Oxford University Press, New York, 1998.
4. L.A. Utracki. Polymer Alloys and Blends, Hanser Publisher, Oxford University Press, New York (1989).
5. J. Finaly; M.J. Hill; P.J. Barham; K. Byrne; A. Woogara. *J Polym Sci Part B* 41, 1384 (2003).
6. M.J. Folkes. Processing, Structure and Properties of Block Copolymers, Elsevier, New York (1985).
7. K. Almdal; K. Koppi. *Macromolecules* 26, 4058 (1993).
8. J.H. Laurer; J.C. Fung; J.W. Sedat; D.A. Agard; S.D. Smith; J. Samseth; K. Mortensen; R.J. Spontak. *Langmuir* 13, 2177 (1997).
9. M.W. Matsen.; F.S. Bates. *Macromolecules* 28, 7298 (1995).
10. F.S. Bates; G.H. Fredrickson. *Physics Today* 52, 32 (1999).
11. K.I. Winey; E.L. Thomas; L.J. Fetters. *J Chem Phys* 95, 9367 (1991).
12. G.H. Frederickson; E. Helfand. *J Chem Phys* 89, 5890 (1988).
13. G.H. Frederickson; E. Helfand. *J Chem Phys* 86, 1553 (1987).
14. P.J. Flory. Principles of Polymer Chemistry, Cornell University Press, Ithaca (1953).
15. F.S. Bates, M. Muthukumar; G.D. Wignall; L.J. Fetters *J Chem Phys* 89, 535 (1988).
16. D.R. Paul, C.B. Bucknall. Polymer blends, John Wiley & Sons, Inc., New York (2000).
17. M.W. Matsen; F.S. Bates. *Macromolecules* 29, 7641 (1996).

18. L. Leibler. *Macromolecules* 13, 1602 (1980).

19. J.D. Londono; A.H. Narten; G.D. Wignall; K.G. Hionnell; E.T. Hsieh; T.W. Johnson; F.S. Bates. *Macromolecules* 27, 2864 (1994).

20. K. Almdal; J.H. Rosedale; F.S. Bates; G.D. Wignall; G.H. Fredrickson. *Phy Rev Lett* 65, 1112 (1990).

21. H. Fried; K. Binder. *Europhys Lett* 16, 237 (1991).

22. R.G. Larson. *Mol Sim* 13, 321 (1994).

23. F.S. Bates; G.H Fredrickson. *Annu Rev Phys Chem* 41, 525 (1990).

24. H. Hasegawa; H. Tamaka; K. Yamasaki; T. Hashimoto. *Macromolecules* 28, 5043 (1995).

25. D.J. Kinning; K.I. Winey; E.L. Thomas. *Macromolecules* 21, 3502 (1988)

26. G.A. McConnell; A.P. Gast; J.S. Huang; S.D. Smith. *Phys Rev Lett* 71, 2102 (1993).

27. S. Foster; A.K. Khandpur; J. Zhao; F.S. Bates; I.W. Hamley; A.J. Ryan; W. Bras. *Macromolcules* 27, 6922 (1994).

28. M.F. Schulz; F.S. Bates. Physical Properties of Polymers Handbook, AIP Press, New York (1996).

29. P. Alexandridis; P. Olsson; B. Lindman. *Langmuir* 14, 2627 (1998).

30. I.W. Hamley; J.P.A. Fairclough; A.J. Ryan; C.Y. Ryu; T.P. Lodge; A.J. Gleeson; J.S. Pedersen. *Macromolecules* 31, 1188 (1998).

31. H. Watanabe; T. Sato; K. Osaki; M.L. Yao; A. Yamagishi. *Macromolecules* 30, 5877 (1997).

32. Information obtained from www.kraton.com

33. J.R. Quintana; E. Diaz; I. Katine. *Langmuir* 14, 1586 (1998).

34. J.R. Quintana; M.D. Janez; I. Katime. *Polymer* 11, 2111 (1998).

35. D.A. Vega; J.M. Sebastian; W.L. Loo; R.A. Register. *Journal of Poly. Sci. Part B* 39, 2183 (2001).

36. R.J. Spontak; N.P. Patel. *Curr Opin Coll Interface Sci* 5, 334 (2000).

37. N.R. Jackson; E.A. Wilder; S.A. White; R. Bukovnik; R.J. Spontak. *Journal of Poly. Sci. Part B* 37, 1863 (1999).

38. T.A. Walker; J.J. Semler; D.N. Leonard; G.J. van Maanen; R.R. Bukovnik; R.J. Spontak. *Langmuir* 18, 8266 (2002).

39. H. Watanabe; S. Kuwahara; T. Kotaka. *J Rheol* 28, 393 (1984).

40. H. Watanabe; T. Sato; K. Osaki. *Macromolecules* 30, 5877 (1997).

41. J.M. Yu; R. Jerome; N. Overbergh. *Macromol Chem Pysic* 11, 3719 (1997).

42. J. Ren; A.S. Silva; R. Krishnamoorti. *Macromolecules* 33, 3739 (2000).

43. N.R. Jackson; E.A. Wilder; S.A. White; R. Bukovnik; R.J. Spontak. *Journal of Poly. Sci. Part B* 37, 1863 (1999).

44. H.J. Walls; M.W. Riley; R.R. Singhal; R.J. Spontak; P.S Fedkiw; S.A. Khan. *Adv Funct Mater* 13, No. 9 (September 2003).

45. R. Krishnamoorti; J. Ren; A.S. Silva. *Journal of Chemical Physics* 11, 4968 (2001).

46. R. Krishnamoorti; R.A. Vaia; E.P. Giannelis. *Chem. Mater.* 8, 1728 (1996).

47. R. Krishnamoorti; E.P. Giannelis. *Macromolecules* 30, 4097 (1997).

48. T.C Meshel; B.D. Freeman; R.J. Spontak; Z. He; I. Pinnau; P. Meakin; A.J. Hill. *Science,* Vol. 0, 2002.

49. T.J. Pinnavaia; G.W. Beall. Polymer-Clay Nanocomposites. Wiley Series in Polymer Science. 2000.

50. R.A. Vaia; E.P. Giannelis. *Macromolecules* 30, 7990 (1997).

51. K.M. Lee; C.D. Han. *Macromolecules* 36, 7165 (2003).

52. B. Hoffman; C. Dietrich; R. Thomann; C. Friedrich; R. Mulhaupt. *Macromol Rapid Commun* 21, 57 (2000).

53. S. A. Khan, N. J. Zoeller. *J. Rheol.* 37, 1225 (1993).

54. E. Theunissen; N. Overbergh; H. Reynaers; S. Antoun; R. Jerome; K. Mortense. *Polymer* 45, 1857 (2004).

Chapter 2: Experimental Procedure

2.1 Definition of a Gel

Gelation is the conversion of a liquid to a disordered solid by formation of a network of chemical or physical bonds between the molecules or particles composing the liquid.[1] A typical gel structure can be seen in Figure 1, where branching plays an important role forming the network (see Figure 2.1).

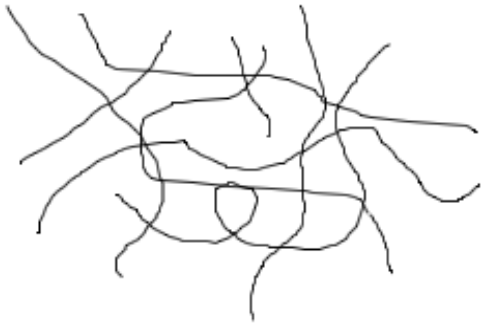

Figure 2.1: Schematic of a gel network

As indicated above, the bonds can be either physical or chemical; there are at least three different types of chemical reactions when forming a chemical polymer gel, **condensation reaction** could be considered the first one; this happens when a polymer molecule has three or more reactive groups, reacting with a cross-linker. **Addition polymerization** happens when a free-radical reaction takes place, allowing the opening of a double bond within the molecule; this creates and additional bond that links monomers

together, leading to a branched structure if there are two or more double bonds. **Cross-linking or vulcanizing** linear polymeric precursors introduce a chemical link that bonds them together.[2] In conclusion, covalent bonds are being formed in chemical gels; these bonds are permanent within certain temperature range. On the other hand, physical gels are a product of the formation of a network composed by weaker bonds due to the presence of van der Waals forces, electrostatic interactions or hydrogen bonds. Physical polymer gels have to have a 3-D network that can be recovered upon thermal cycling and should be the minor component in a matrix where liquid is the major component.[3]

2.2 Rheology

Rheology can be defined as the science of flow and deformation of materials. To determine the consistency of a material both its viscosity and elasticity parameters must be studied; the viscosity of a material is related to its resistance to flow, while the elasticity is related to its degree of structure. A rheometer measures the rheological properties as a function of rate or frequency of deformation; for example, a rheometer imposes a shear flow on a system and it measures the resulting stresses or, it could impose a shearing stress and measure the resulting shearing rate.[1]

Different flow geometries exist in order to impose a shearing flow: sliding plates, concentric cylinders, cone and plate, parallel disks, capillary, slit flow and axial annulus flow. Parallel plates (see Figure 2.2) was the chosen geometry for this project; cone and plate could have also been chosen but, for viscosities exceeding 10^3 Pa.s (the samples studied have viscosities of approximately 6.10^3 Pa.s and higher) and high elasticity, edge

failure is a severe limitation. Not only that, trying to "squeeze" samples, like the one being studied, into a conical shape is very hard; while with parallel plates, samples can be molded or cut into small circles from sheets, obtaining data within minutes of loading the sample. Parallel plates are also recommended for time dependent studies, like stress relaxation.[4]

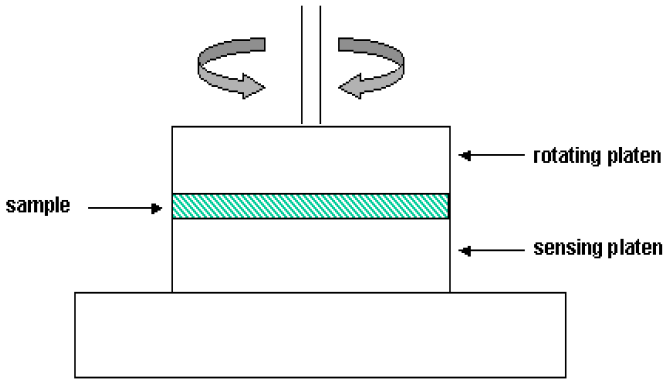

Figure 2.2: Schematic parallel plates

Before continuing talking about shear stress, shear strain and shear rate one should know what happens in a system under shear. Consider a small cubical volume of material. Under the action of forces that produces shear stress, the shape shifts to a parallelogram. Figure 3 shows such a volume at rest and immediately following application of force. The change in shape has two components, elastic deformation E and slippage S. The elastic deformation is accompanied by storage of elastic energy within the structure of the material, while the slippage is associated with a continuous input of viscous energy. When the force is removed, the deformed material undergoes a partial recovery of shape as the elastic energy is recovered; the shape change due to slippage is permanent. Thus, in steady

flow the displacement component S continues to increase and measurements of the non-time-varying force and velocity provide no information about the elastic energy component. In a time-varying flow, however, the elastic energy component also varies with time and may be either increasing or decreasing, while the viscous energy is always increasing. Consequently, the relation between the time-varying force and velocity reflects both the elastic and viscous properties of the material.[5]

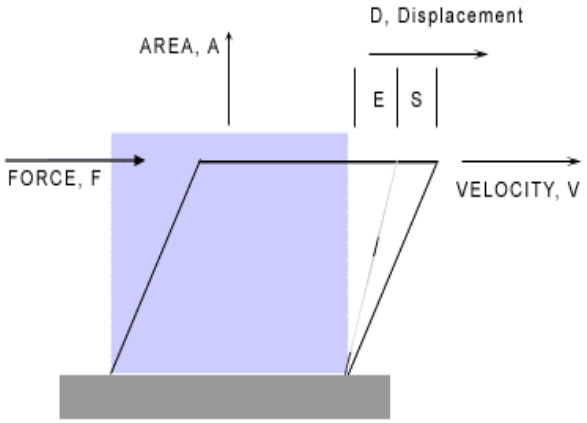

Figure 2.3: Schematic of a small cubical volume under shear[5]

Figure 3 can also be used for defining the shear stress, shear strain and shear rate. "H" is the height of the cubicle volume in Figure 3

Shear Stress: $\sigma=F/A$ (Equation 1)

Shear Strain: $\gamma=D/H$ (Equation 2)

Shear Rate: $\dot{\gamma}=V/H$ (Equation 3)

Shear stress, σ, can be defined as the force that a flowing liquid exerts on a surface, per unit area of that surface, in the direction parallel to the flow.[1] Based on this, shear viscosity can be defined as

$$\eta = \sigma/\gamma \quad \text{(Equation 4)}$$

Small amplitude oscillatory shearing allows the study of structural rearrangements without significantly deforming the system microstructure (this translates into small strain amplitude, $\gamma_0 << 1$). An oscillatory shear strain of angular frequency ω is going to be generated in the system:

$$\gamma = \gamma_0 \sin \omega t \quad \text{(Equation 5)}$$

The stress response to this oscillatory strain, assuming a linear viscoelastic system, is also going to be sinusoidal, but is out of phase with the strain by δ.[6] The stress measured during this oscillatory deformation, is controlled by the rates of spontaneous rearrangements, or relaxations, present in the system in the equilibrium state.[1] The sinusoidal stress response can be represented as

$$\sigma(t) = \gamma_0[G'(\omega) \sin(\omega t) + G''(\omega)\cos(\omega t)] \quad \text{(Equation 6)}$$

G’(ω) is considered the real part of the modulus and it is known as the storage modulus (representing storage of elastic energy) while G’’(ω), is considered the imaginary part and it is known as the loss modulus (representing the viscous dissipation of that energy).[6]

There could be different rheological responses, depending on the nature of the system. In the presence of a solid-like system the steady-state shear stress is independent of shear rate and the shear viscosity decreases with increasing shear rate;[1] from a modulus (G’ and G’’) point of view, G’ >> G’’ and G’ is frequently independent. While in the presence of a “liquid like” system, there is no shear thinning (the viscosity is constant) and the stress increases linearly with shear rate; in the case of low frequency, there is a region, called the terminal region, where G’ and G’’ obey power laws.[1]

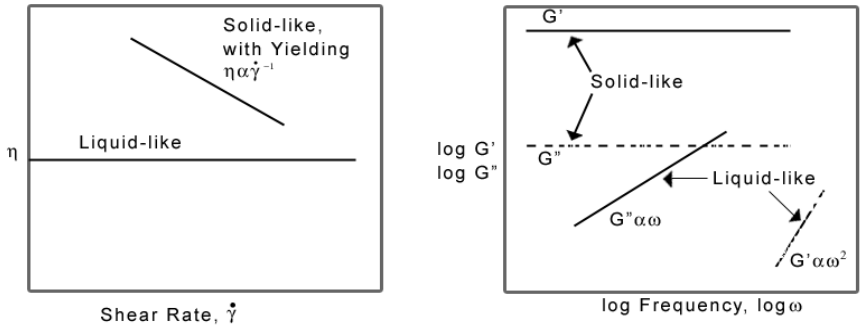

Figure 2.4: Comparison between “liquid-like” and “solid-like” behavior[1]

The viscoelastic properties of the gels were analyzed by dynamic rheology performed on a Rheometrics dynamic stress rheometer and an ATS RheoSystem Stresstech rheometer, operated with either, 20 or 25 mm parallel plates and 1.2 or 2.0 mm gap heights. Values of the dynamic storage and loss modulus (G’ and G”) were recorded at

ambient temperature as functions of shear stress (τ) and oscillatory frequency (ω=1rad/s) in the linear viscoelastic limit.

The rheological response of physical gels falls in the solid-like behavior mentioned above. The storage modulus is nearly frequency (ω) independent, G'>>G'' at least by a couple order of magnitude and the complex viscosity decreases as the shear rate increases. This behavior has been reported plenty of times.[7-10]

By changing the temperature, the system can go through an order – disordered transition, or vice versa, at a thermodynamically precise temperature. This transition is characterized by a significant loss in the elastic modulus and crossing of G' and G'' (Bates Method). Dynamic rheological test were performed with parallel plates separated by either, a 2 mm or 1.5 mm gap on an ATS RheoSystems Stresstech rheometer. Measurements were conducted under a nitrogen purge over temperature intervals ranging from 30°C to as high 200°C in 3°C increments with a 2 min dwell time at each temperature. The strain amplitude (γ_0) and oscillatory frequency (ω) during these tests were held constant at 2.0% and 1 rad/s which are within the linear viscoelastic limit.

2.4 Stress Relaxation

Materials of different nature, silk, gum rubber, glass, can exhibit time dependence in their elastic response. An instantaneous deformation, as expected for a Hookean solid, followed by a continuous deformation, has been seen when a load, in shear or extension, is applied on the materials mentioned above and others; this time-dependent response is

known as viscoelasticity. Stress relaxation and creep are the most common methods used to measure this phenomenon.

Scientists, in order to understand viscoelasticity, have developed different theories by using spring coils and dashpots. The most known ones are Maxwell's, where a spring (which represents elastic behavior) and a dashpot (which represents viscous behavior) are in series, Kelvin's, where a spring and a dashpot are in parallel and Zener's, where he combined a spring with either Maxwell's or Kelvin's. Zener's model has been, so far, the best model used to explain and understand linear viscoelasticity; it only assumes two characteristic times, one associated with creep and the other, associated with stress relaxation.

When a polymeric liquid is subject to a step increase in strain, the stress relaxes in an exponential fashion. Now, if a purely viscous liquid is subjected to the same deformation, the stress relaxes instantly to zero as soon as the strain becomes constant. An elastic solid would show no relaxation.

The relaxation modulus relates stress, as a function of time, with strain.

$$G(t) = \tau(t)/\gamma_0 \quad \text{(Equation7)}$$

In the presence of polymeric systems, all the data for small strains fall on the same curve. At short times the relaxation modulus approaches a constant value known as the plateau modulus G_e; this linear dependence, of stress relaxation on strain, is known as linear viscoelasticity.

At very short times G (t) tends towards the limiting value of G_U and, at very long times, G (t) tends towards G_R; where U and R stand for Unrelaxed and Relaxed. In these extreme regions the shear becomes more and more elastic, independent of time.[6]

Crosslinked rubber shows a short time relaxation followed by a constant modulus; concentrated suspensions exhibit the same behavior but only at very small strains. High molecular weight concentrated polymeric liquids show behavior similar to rubber at shorter times with a nearly constant modulus plateau G_0, eventually followed by flow at long times.[4]

Stress relaxation exoperiments were performed in a Rheometrics Mechanical Spectrometer RMS800, using 25 mm parallel plates separated by a mean gap size of either 1.5 mm or 2 mm. The strain amplitude (γ_0) and oscillatory frequency (ω) during these tests were held constant at 0.1% and 1 rad/s which are within the linear viscoelastic limit.

2.5. Scanning Electron Microscopy (SEM)

All Scanning Electron Microscopes consist of a column which generates a beam of electrons, a specimen chamber where the electron interacts with the sample, detectors to monitor the different signals that result from the electron beam/sample interaction and a viewing system that builds an image from the detector signal.

The electron column consists of an electron gun and two or more electron lenses. The electron gun, which could be either a thermionic or a field emission source, is responsible for the production of electrons and the acceleration of these, to a range of 1 – 40 keV.

These electrons, coming out of the gun, produce a beam with large diameter. Before continuing, it is important to know that the final beam diameter, also known as the spot size, plus the amount of current in the final probe, limits the image resolution in the SEM; that is why operators have to play with different parameters, until the "right combination" of parameters is found, in order to obtain high quality images. Electron lenses are used to reduce the diameter of the beam coming out of the gun, placing a small focused electron beam on the specimen. This results in an interaction between the beam and the near-surface region of the specimen up to certain depth (1-2 μm) and generates signals used to form an image (see Figure 2.5).

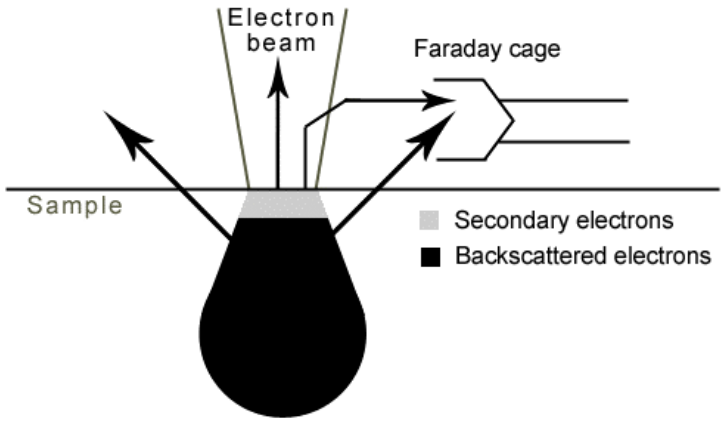

Figure 2.5: Signals obtained from the Interaction Volume[11]

The deflection system is responsible for scanning the beam along a line and then displace the line position for the next scan so that a rectangular raster is generated on both the specimen and the viewing screen.[11] Two pairs of deflection coils are responsible for the raster of the beam. Magnification is defined as the ratio between the linear size of the viewing screen to the linear size of the raster on the sample. High magnifications are

obtained when a smaller raster width appears larger when displayed on the viewing screen.[11]

The two signals most often used to produce images are Secondary Electrons (SE) and Backscattered Electrons (BSE); these are collected by an Everhart – Thornley (E – T) detector composed by a scintillator, a light pipe, and a photomultiplier tube. The E-T detector is located to the side of the specimen and has a wire mesh screen in front of it, which could either have a positive or a negative potential; the potential depends on the type of electrons the operator wants to draw from anywhere in the specimen chamber. A positive potential (around +300V) is used in order to draw SE and a negative potential (around -100V) is used to draw BSE; although BSEs are more efficiently collected by an overhead backscatter detector, they can also be collected by an E – T detector. Once the electrons "get inside" the E – T detector, they are going to be accelerated by a positive potential, around +12 kV, causing the emission of lights every time they hit the scintillator walls; this light is going to travel down a light pipe until it gets to the Photo Multiplier Tube (PMT), where the light is converted into an electrical signal. The intensity changes that can be seen on the viewing screen are a product of the variations in signal as the beam moves over the sample's surface.[11]

2.6.- Transmission Electron Microscopy (TEM)

In Transmission Electron Microscopy a coherent beam of mono-energetic electrons is created by a thermoionic or a field emission source, being referred to as an electron gun. The electron beam is then focused onto a thin specimen by a series of electromagnetic lenses. So far, TEM sounds a lot similar to SEM but, there is a big difference between the two of them; starting with the final probe size, SEM can resolve down to ≈ 2nm, while TEM can resolve down to 2 Å, having a higher lateral spatial resolution than SEM. In terms of energy spread (ΔE), variation of electron energies leaving the filament to form the beam, SEM can have values as low as 0.3 eV, while TEM can have 0 eV (10). TEM also has the ability of collecting both, imaging and diffraction information from the same area of a specimen (see Figure 7); when the focused electron beam is on an area of the thin sample, interaction between the beam and the potential field of an atomic nucleus takes place. This interaction also extends to the electron cloud that surrounds the nucleus. If some of the energy of the incident electron is lost through a scattering event, the scattering is considered to be inelastic; while, if there is no loss in energy, the scattering is considered elastic. When the electrons of the probe enter the specimen, they are in phase; their phase relationship is altered upon exiting the specimen, this alteration upon exiting the sample can be correlated with the spatial association between scattering centers. The sensitivity to slight perturbation in the atomic structure of the sample makes TEM and extremely powerful imaging tool.

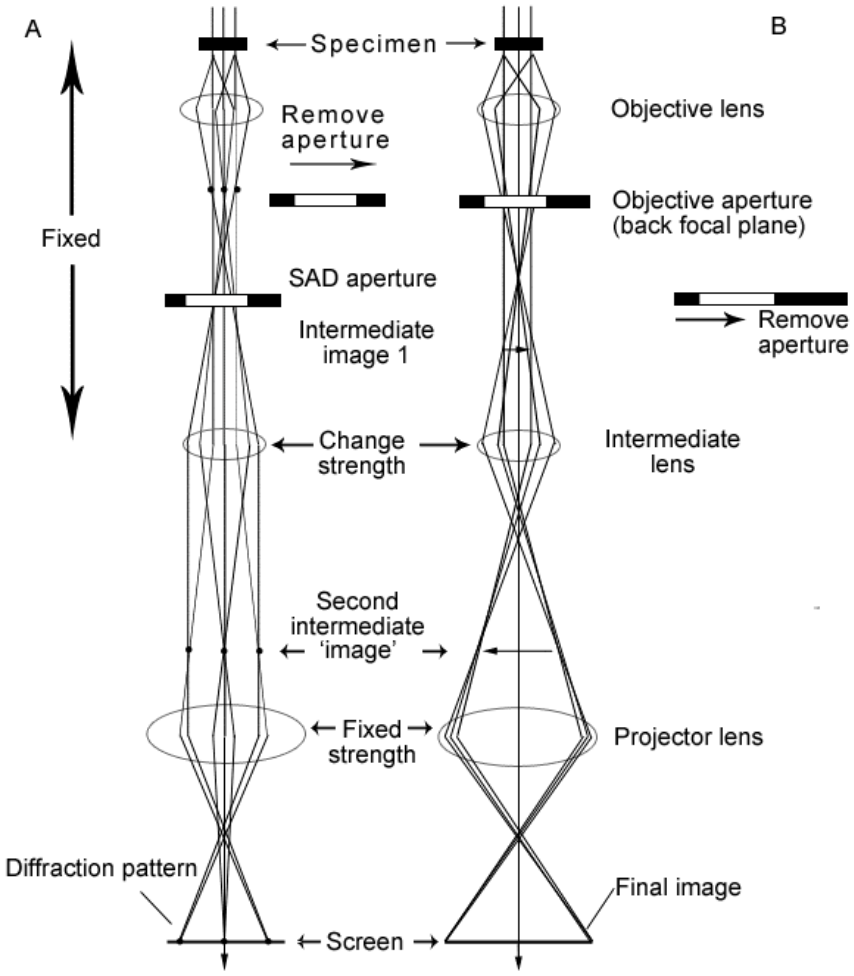

Figure 2.7: The operating modes of TEM[12]

As indicated above, there are two "operation modes" in a TEM. If an electron diffraction pattern from the "illuminated area" of the specimen is needed, the TEM has to be operated in diffraction mode. The objective lens takes the electrons emerging from the "exit surface" of the sample and disperses them to from a diffraction pattern; the post

specimen lenses are adjusted to examine the information in the transmitted signal at the back focal plane of the objective lens. A final diffraction pattern can be displayed by projecting the electron waves onto a viewing screen within the microscope column. If an image of the "illuminated area" is desired, the TEM has to be operated in imaging mode. The objective lens takes the electrons emerging from the "exit surface" of the sample and recombines them to form an image in the imaging plane; the post specimen lenses are set to examine the information in the transmitted signal at the image plane of the objective lens and at this point the scattered electron waves are finally recombined, forming an image created from the sample microstructure that is finally displayed onto a viewing screen within the TEM column.[12]

Bulk gels were sectioned at -100°C in a Reichert-Jung cryoultramicrotome to produce electron – transparent specimens for TEM. The sections were exposed to the vapor of 0.5% RuO_4(aq) for 7 min to stain phenyl containing moieties. Images were acquired on a Zeiss EM902 electron spectroscopic microscope operated at 80 kV and 0eV energy loss.

2.7 X-Ray Diffraction (XRD)

Diffraction is a great technique for obtaining knowledge about the spatial arrangements of atoms in materials. An incident wave is directed into a material and a detector is typically moved about to record the directions and intensities of the outgoing diffracted waves.[12] Constructive or destructive interference can occur along different directions, due to the interaction of scattered waves emitted by atoms of different types and positions. Diffraction at small angles is due to atomic periodicities with long repeat distances, while

diffraction at high angles is due to short repeat distances (small inter-planar spacing). Sharp and clear diffraction patterns is a typical characteristic of crystals with precise periodicities over long distances, while amorphous materials show diffraction patterns that lack sharp diffraction peaks; although the pattern lacks of defined peaks, diffraction is also used to study the structure of amorphous materials.[12]

The incident waves must have wavelengths comparable to the space between atoms. The electric field of the incident X-Ray moves the atomic electrons and their acceleration generates an outgoing wave. Bragg was the first one to prove this; in Bragg's law, the angle of incidence of the two parallel rays is θ and *d* is the interplanar spacing which, sets the difference in path length for the ray scattered from the top plane and the ray scattered from the bottom plane.[13]

The difference in path lengths is $2d\sin\theta$; strong diffraction, constructive wave interference, occurs when the difference in path length for the top and bottom rays is equal to one wavelength λ

$$2d\sin\theta=\lambda \quad \text{(Equation 8)}$$

People have compared physical gels with glasses, disordered solids formed by the progressive freezing of some of the liquid degrees of freedom as the temperature is lowered.[1] The mobility of the polymer molecules is quenched due to the formation of a network of bonds that relaxes slowly, if at all. Regularity in the arrangements of atoms is absent up to certain degree, not being completely disordered. Lets considered a collection of macromolecules, where all the atoms are linked by a succession of chemical bonds with

fixed lengths and angles. The purely atomic density distribution, P(r), will have the highest value when, r corresponds to the bond length r_o of the most common bond type in the system; P(r) will oscillate in the vicinity of r_o. Due to this oscillation, the scattering pattern will result in a typical diffuse halo.[13]

2.8 References

1. R.G. Larson. The Structure and Rheology of Complex Fluids, Oxford Unviersity Press (1999).
2. R.J. Young; P.A. Lovell. Introduction to Polymers, Chapman & Hall, 2nd edition (1991)
3. D.J. Mercurio, R.J. Spontak. *J Phys Chem B* 11, 2091 (2001)
4. C.W. Macosko. Rheology Principles, Measurements and Applications, Wiley-VCH (1994)
5. G.E. Dieter. Mechanical Metallurgy, Mc Graw-Hill, 3rd edition (1986)
6. N.G. McCrum; C.P. Buckley; C.B. Bucknall. Principles of Polymer Engineering Oxford University Press, 2nd edition (1997)
7. H. Hoffmann; T. Durrschmidt. *Colloid Polym Sci* 279, 1005 (2001)
8. J.H. Laurer; S.A. Khan; R.J. Spontak. *Langmuir* 15, 7947 (1999)
9. N.R. Jackson; E.A. Wilder; S.A. White; R. Nukovnik; R.J. Spontak. *J Polym Sci Part B* 37, 1863 (1999)
10. K. Mortensen; E. Theunissen; R. Kleppinger; K. Almdal; H. Reynaers. *Macromolecules* 35, 7773 (2002)
11. J.I. Goldstein et al. Scanning Electron Microscopy and X-Ray Microanalysis, Plenum Press, 2nd (1992)
12. B. Fultz; J.M. Howe. Transmission Electron Microscopy and Diffractometry of Materials, Springer Edit. (2001)

13. M. Kakudo; N. Kasai. X-Ray Diffraction by Polymers. Elsevier Publishing (1972) Company

Chapter 3: ABA Triblock Copolymer Gels Modified with an A-Compatible Semicrystalline Homopolymer

3.1 Abstract

In the presence of a midblock-selective solvent, ABA triblock copolymers form physical gels in which bridged and entangled B-chains establish a swollen network stabilized by A-microdomains. Here, we seek to improve the properties of an ABA gel through the addition of an A-compatible, high-molecular-weight semicrystalline homopolymer (shA).

Dynamic rheology indicates that the elastic modulus increases substantially, and far beyond that achievable with an inert filler, with increasing shA content at constant solvent concentration. Transmission electron micrographs reveal the existence of nanoscale shA filaments and sheets dispersed in a micelle-stabilized gel network. The shape of the nanoscale shA objects, which are partially crystalline according to differential scanning calorimetry, and their apparent interaction with the A-rich micelles enhance network development and are responsible for the pronounced modulus increase.

3.2 Introduction

Block copolymers can spontaneously order into a variety of nanoscale structural elements[1-3] and impart complementary properties to multifunctional materials. While such ordering may occur in the molten or solvated state, we focus our attention exclusively on

block copolymers in the presence of a liquid solvent.[4] Lodge and co- workers[5] have investigated the phase behavior of AB diblock copolymers in a neutral solvent and have demonstrated that all the morphologies observed in molten block copolymer systems can likewise be induced in an AB copolymer upon addition of a solvent. Since neutral solvent molecules distribute uniformly within the A- and B-rich microdomains of the copolymer, they screen enthalpic A/B interactions, resulting in a diluted system6 that can be ultimately forced to disorder.7 Selective solvents, however, predominantly swell only thermodynamically compatible microdomains and, at sufficiently high concentrations, induce changes in interfacial curvature and, hence, morphology.

A vast array of morphologies is evident in the elegant ternary phase diagrams reported[8] for ABA triblock copolymers derived from poly(ethylene oxide) and poly(propyleneoxide) in the presence of two selective solvents, but only binary triblock copolymer/solvent systems are considered further. By examining the composition dependence of styrenic triblock copolymers in a midblock-selective solvent, Laurer et al.[9] have shown that the lamellar, cylindrical, and spherical morphologies can be generated by varying solvent concentration. Within the spherical (micellar) regime, solvent concentration has a pronounced effect on rheological properties due to the degree to which the micelles order on a cubic lattice and the spatial arrangement of the copolymer molecules under given deformation conditions.[10-14] At relatively high copolymer concentrations (C), the bridged and looped conformations adopted by copolymer midblocks contribute to the plateau modulus (G_0): bridges form a physical network that connects A-rich micelles, and loops promote entanglement. Vega et al.[15] have proposed that entanglements dominate the magnitude of G_0, with $G_0 \approx C^n$ and $n \approx 2$ for S-endblocked copolymers. Under these conditions, the copolymer molecules form a

physical gel in which swollen midblocks are physically cross-linked by glassy S-rich micelles (see Figure 3.1).[9,16]

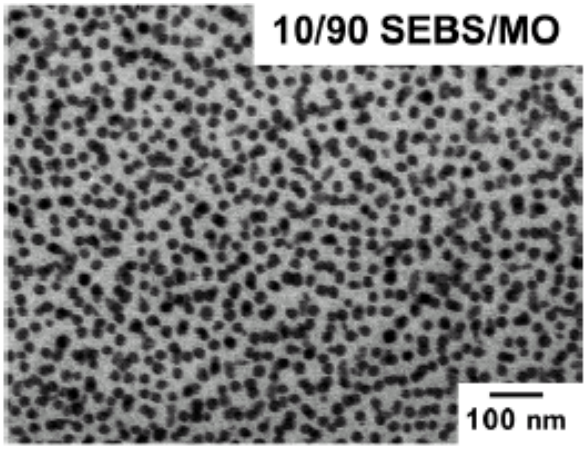

Figure 3.1: Transmission electron micrograph of a block copolymer gel composed of 10 wt % SEBS and 90 wt % mineral oil (MO).15 The S-rich micelles appear dark due to selective staining.

Dielectric measurements[17] confirm that the extent to which the midblocks form bridges decreases as C decreases. At copolymer concentrations just above the critical gelation concentration (in the Rouse limit), only bridged midblocks contribute to G_0, which scales[10] as C.

Physical attempts reported in the open literature to tune the mechanical properties of styrenic triblock copolymer gels without varying C have employed S-compatible homopolymers to swell the micellar cores,[18-20] as well as diblock copolymers to modify the extent to which midblocks connect neighboring micelles and form networks. [15,21,22] Novel

processing techniques have likewise been developed for this purpose.[23,24] While alternative physical modification strategies (e.g., addition of matrix modifiers, such as paraffinic wax or a polyolefin) are available in the patent literature, they are not considered further, since the objective here is to explore modified gels in which the additive is S-compatible. In the present work, we investigate the rheological, morphological, and thermal properties of styrenic triblock copolymer gels modified through the addition of a semicrystalline S compatible homopolymer.

3.3 Experimental Section

3.3.1. Materials

A commercial poly[styrene-b-(ethylene-co-butylene)-b-styrene] (SEBS) triblock copolymer with 31 wt % S and a molecular weight (M) of 161 000 (Kraton G1654) was used to prepare the gels investigated here. The midblock-selective solvent was the same aliphatic mineral oil (MO) from Witco Corp. (Hydrobrite 380) described previously.9,16,19 Syndiotactic homopolystyrene (shS) with M) 250 000 was obtained from Dow Chemicals (Questra QA100) and used as-received. Reagent-grade toluene was purchased from Aldrich Chemicals.

3.3.2. Methods.

A series of block copolymer gels containing 90 wt% mineral oil was prepared by separately dissolving predetermined amounts of SEBS copolymer, shS, and MO in an excess of toluene at its boiling point. The concentrations of SEBS and shS were varied so that the mass percent of shS (wshS) ranged from 0.00 to 1.47 in the final SEBS/shS/MO gels. Upon dissolution of the SEBS and shS, a set of SEBS/toluene and MO/toluene solutions was combined and mixed. The complementary shS/ toluene solution was then added, and the resulting SEBS/shS/ MO/toluene solution was poured into a mold at ambient temperature. Similarly, SEBS/shS blends (without MO) were prepared for thermal analysis. Once the solutions were cool, they were kept in a fumehood for 3 days and later stored under vacuum at 60 °C for another 3 days to remove residual traces of toluene. The viscoelastic properties of the gels were analyzed by dynamic rheology performed on a Rheometrics dynamic stress rheometer and an ATS RheoSystems Stresstech rheometer, operated with either 20 or 25 mm parallel plates and 1.2 or 2.0 mm gap heights. Values of the dynamic storage and loss moduli (G' and G'', respectively) were recorded at ambient temperature as functions of shear stress (τ) and oscillatory frequency (ω) in the linear viscoelastic limit. Bulk gels were sectioned at -100 °C in a Reichert-Jung cryoultramicrotome to produce electron-transparent specimens for transmission electron microscopy (TEM). The sections were exposed to the vapor of 0.5% RuO4 (aq) for 7 min to stain phenyl-containing moieties. Images were acquired on a Zeiss EM902 electron spectroscopic microscope operated at 80 kV and 0 eV energy loss. Differential scanning

calorimetry (DSC) of SEBS/shS blends and SEBS/shS/MO gels was performed on a Perkin-Elmer DSC-7 instrument operated at 10 °C/min.

3.4 Results and Discussion

The frequency spectra of G' and G'' measured from the SEBS/MO systems with and without shS are presented in Figure 2a and indicate that these systems behave as physical gels. This classification refers to a liquid-rich system exhibiting solid-like character, as signified by the following characteristics:[25] (i) G' exceeds G'' over all ω, and (ii)G' is independent of ω. Confirmation of gel behavior is important, since the concentration of SEBS is reduced as wshS is increased (so that the total polymer content remains constant at 10 wt %). At sufficiently low copolymer content (below the critical gel concentration), gel behavior is no longer retained due to insufficient network formation.

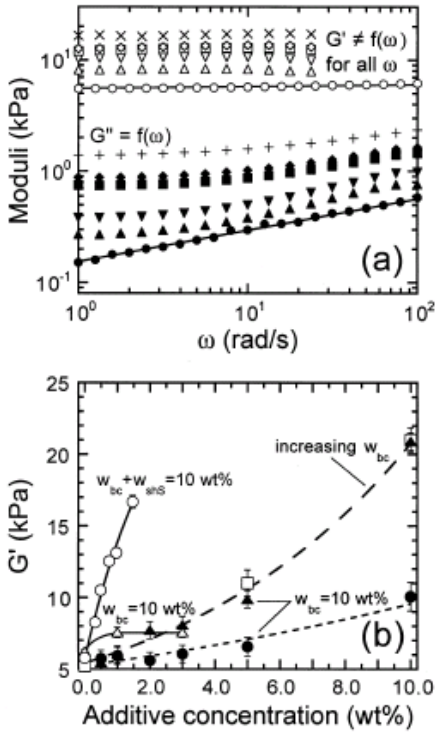

Figure 3.2: Influence of additives on the dynamic mechanical properties of SEBS/MO gels. In part a, the spectra of G' (open symbols) and G'' (filled symbols) are displayed for gels with varying concentrations of shS (wshS, in wt %): 0.00 (circles); 0.32 (triangles); 0.49 (inverted triangles); 0.75 (squares); 0.97 (diamonds); 1.47 (x, G'; +, G''). The solid lines are power-law fits to the data for the unmodified gels. In part b, G' is presented as a function of additive concentration for three polymers: shS (open circle); PPO (open triangle); SEBS (open square). Included for comparison are data from gels filled with colloidal silica (b) and a montmorillonite organoclay (2). The mass percent of SEBS (w_{bc}) in each series is identified in the figure. Error bars denote one standard deviation in the data, and the lines (solid and dashed) serve as guides for the eye.

While G'' appears to be weakly dependent on – in Figure 2a, this relationship is not of further interest here. Mean values of G' are presented as a function of additive concentration (wt% shS in the case of the present gels) in Figure 2b and reveal that incorporation of shS into SEBS/MO gels increases the magnitude of G¢ substantially (by almost a factor of 3x as wshS is increased from 0.00 to 1.47 wt %). Included for comparison in Figure 2b are data reported[19] for SEBS/MO gels modified with poly(2,6-dimethylphenylene oxide) (PPO), which is S-compatible. Addition of PPO to SEBS/MO gels at constant copolymer content (10 wt %) initially promotes an increase in G' due to swelling of the S-rich micelles, but this effect is not nearly as striking as that in the present SEBS/shS/MO gels. A substantial, albeit less notable, increase in G' can likewise be achieved by simply adding a solid nanoscale filler to the gel matrix. Data acquired from SEBS/MO gels modified with either colloidal silica particles (ca. 20 nm mean diameter) or a platelike organoclay (a montmorillonite modified with a ternary ammonium salt composed of hydrogenated tallow) are displayed in Figure 2b to establish baseline improvements afforded by inert nanofillers differing in morphology.26 While the magnitude of G' increases with increasing concentration of either filler (the organoclay promotes a more pronounced increase in G' than the colloidal silica), neither filler is as effective at enhancing G' as shS. Also shown in Figure 2b is the dependence of G' on increasing SEBS copolymer content. In this case, no additive corresponds to 10 wt% copolymer, whereas 10 wt % additive refers to 20 wt % copolymer. These data[16] demonstrate that G' increases with increasing copolymer content, scaling as $C^{2.43}$, to the same extent as that for the organoclay-modified gels. According to the results provided in Figure 2b, the increase in G' induced by the addition of 1.47 wt % shS is achieved with

about 8.4 wt % SEBS. Such an increase in copolymer content decreases the intermicellar spacing, promotes micellar ordering, and facilitates the formation of midblock bridges and entangled loops. Since shS cannot alter the magnitude of G' by this mechanism, the role of shS in gel modification must be ascertained. For this purpose, we now turn our attention to the morphology of SEBS/shS/MO gels.

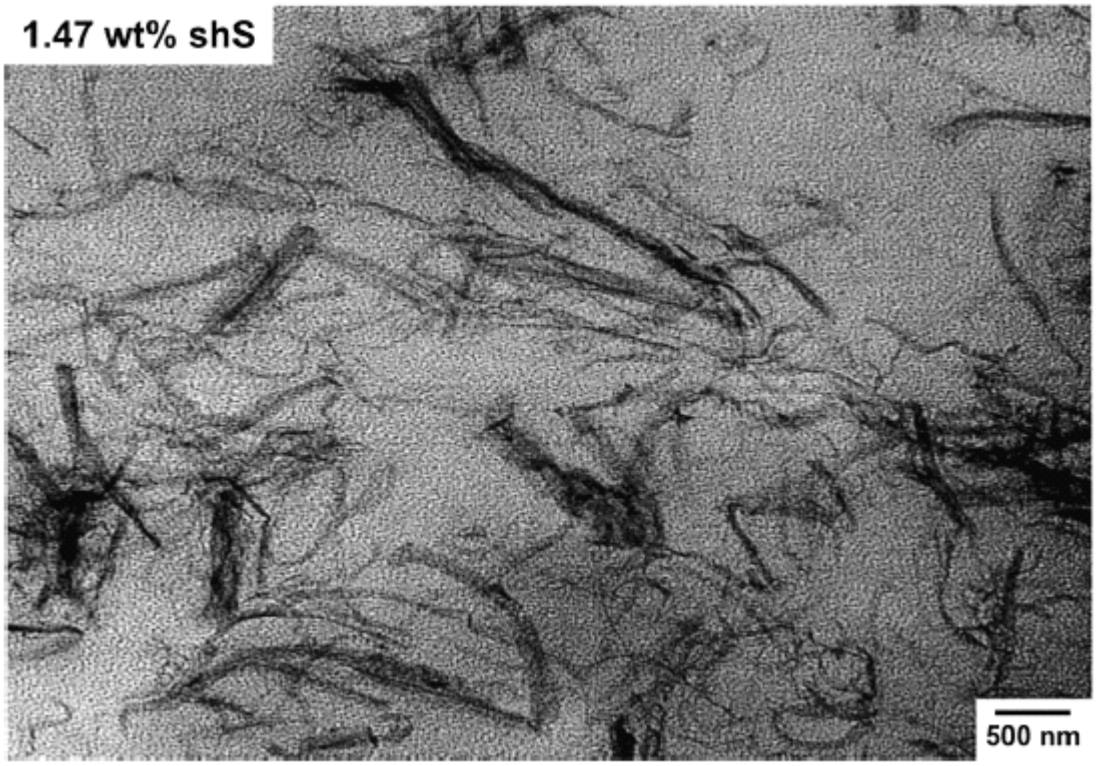

Figure 3.3: TEM image of the SEBS/MO gel with 1.47 wt % shS. Nanoscale shS filaments and sheets appear dark due to RuO4 staining. The SEBS micellar network is visible in the background.

Figure 3.3 displays a representative TEM image of a gel with 1.47 wt % shS. The electron-opaque (dark) features identify RuO4-stained S moieties in the SEBS copolymer and the added shS. Close examination of this image reveals the presence of S-rich micelles measuring about 15 nm in diameter, which is slightly smaller than the 21 nm reported earlier16 for melt-mixed SEBS/MO gels. This difference in micelle size cannot, however, explain the measured increase in G' with increasing wshS evident in Figure 2b. Because of its high molecular weight relative to the S-endblocks of the SEBS copolymer, the shS macrophase-separates from the copolymer and forms an intricate network of nanoscale filaments and sheets differing in thickness, length, and shape. Some of these features measure up to a couple of micrometers in length and down to approximately one micelle diameter in width. To put these dimensions in perspective, the length of a fully extended shS chainof M = 250 000 is estimated from $N_s l_s$ (NS = M/mS, with m_S = 104, and l_S = 0.70 nm) to be about 1.7 μm. Thus, the elongated objects visible in Figure 3 may correspond to highly extended bundles of shS molecules. Alternatively, at high shS concentrations, some objects most likely represent chain folded shS lamellae that crystallize during sample preparation. Scrutinization of the shS features is facilitated by the higher magnification images of the gel with 0.25 wt% shS presented in Figure 4. Figure 4a shows several shS structural elements dispersed throughout the SEBS micellar network. The two sheet-like objects on the left are relatively dark, indicating that they are thick, as well as stained. The seemingly closed-loop object near the top of the image and the shS strings in the lower left corner confirm that some of the shS objects are remarkably flexible. While the shS sheet identified by the arrow is thin and highly electron-transparent, the thicker (darker) sheet below is likewise sufficiently transparent to permit

visualization of the S-rich micelles either above, below, or on the sheet (see the enlargement). Similar morphological characteristics are observed in Figure 4b and c. In Figure 4b, thin shS sheets appear as filaments along their periphery (see arrow) and exhibit evidence of twist (see arrowhead). Some of the filaments or sheets seen edge-on measure about one micelle diameter thick and appear to connect adjacent micelles. While such nanoscale features are interesting, their effect on G' must be established.

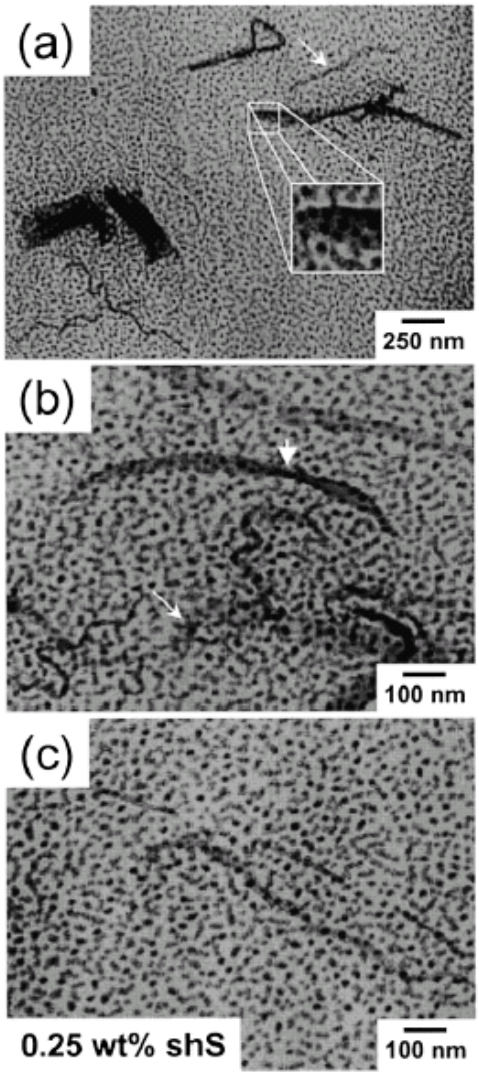

Figure 3.4: Series of TEM images showing the shS nanostructural elements in the SEBS/MO gel with 0.25 wt% shS. In part a, the arrow identifies a thin shS sheet, and the enlargement demonstrates the transparency of a thicker sheet. In part b, the arrow shows where a thin shS sheet appears to connect to a thread, whereas the arrowhead indicates evidence of twist in another sheet.

On the basis of the rheological measurements in Figure 2 and the nanostructural elements visible in Figures 3 and 4, we propose that the shS molecules form nanoscale aggregates, crystals, or a combination of both that physically interact with the copolymer micelles and provide nanoscale reinforcement of the block copolymer gels. Two possible scenarios by which this could be achieved are depicted inScheme1, in which micelles either form along shS filaments or adsorb on the surface of shS sheets.27 In both cases, the added shS would serve to enhance the overall connectivity of the micellar network due to interfacial adhesion to the S-rich micelles and ultimately increase the solid-like character of the gel. While indisputable proof of such interaction is not yet available, our proposed explanation is consistent with recent surface force measurements28 that reveal a substantial increase in the viscosity of solutions composed of surface-adsorbed micelles. Moreover, the observation that G' at a given filler concentration is substantially higher for shS than for an inert filler (particulate or platelike[26]) further supports the likelihood of physical interaction between shS molecules and the S blocks of the copolymer. The extent to which either of our two proposed scenarios occurs is expected to be sensitive to shS dispersion and copolymer micellization, which are, in turn, strongly dependent on specimen preparation conditions and, more specifically, the interplay between toluene evaporation and cooling-induced polymer crystallization/micellization. Another consideration not to be overlooked is that deformation of the gel may likewise be impeded (and G' increased) if some of the long shS filaments and sheets are relatively rigid (glassy or semicrystalline).

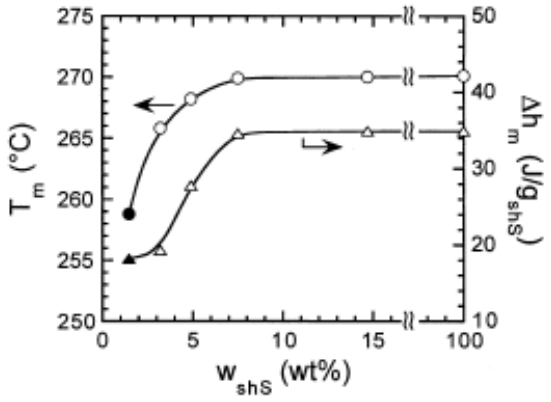

Figure 3.5: Dependence of the shS melting point (Tm, circles) and specific heat of melting (Δh_m, triangles) on wshS. Data collected from SEBS/shS blends and SEBS/shS/MO gels are denoted by open and filled symbols, respectively, and the solid lines serve as guides for the eye.

Results obtained from DSC for SEBS/shS blends and one SEBS/ shS/MO gel are provided in Figure 5 and reveal that the melting point (Tm) and heat of melting (Δh_m) of shS decrease measurably when the concentration of shS falls below _7 wt %. In particular, the value of Tm in the gel with 1.47 wt % shS is about 11 °C lower than that of the neat homopolymer, indicating a slight reduction in crystalline perfection. The corresponding value of Δh_m, however, is about 48% lower than that of neat shS, confirming that only about half of the chains that crystallize in the neat homopolymer form chain-folded lamellae in the gel. Repeated attempts to identify a melting endotherm in the gels with lower shS content have failed due to either insufficient instrument sensitivity or the absence of crystalline shS.

3.5 Conclusions

Addition of high-molecular-weight shS to a micellar SEBS/oil gel at constant oil content serves to reinforce the gel, as evidenced by a pronounced increase in G'. This increase reflects the formation of nanoscale shS filaments and sheets that are uniformly dispersed throughout the gel matrix. These nanostructural elements differ in size and shape, and measure as thin as one micelle diameter. Thermal analysis of the gel possessing the highest shS concentration reveals that some of these elements are crystalline, most likely arranged as chain-folded lamellae. Because of their size, shape, dispersion, and compatibility with the S blocks of the copolymer molecules, the nanoscale shS objects can contribute to the magnitude of G¢ through a combination of their selective interaction with the S-rich micelles and their intrinsic resistance to mechanical deformation. Comparison of results obtained from comparable shS- and silica-modified gels confirms that the shS is far more effective in improving gel stiffness than an inert filler, which is consistent with the likelihood of physical interaction between the nanoscale shS objects and the S-rich micelles. The results presented here demonstrate that the properties of ABA block copolymer solutions may be controllably and substantially modified through the addition of an A-compatible semicrystalline polymer.

3.6 Acknowledgment

We thank the Distance Education program at NC State University for partial financial support, Dr. S. A. Khan and Dr. C. R. Daubert for the generous use of their

rheometers, Ms. S. L. Seeley and Ms. J. E. Stevens for technical assistance, and Dr. E. Kumacheva (University of Toronto) for insightful discussions.

LA026117D

3.7 References

1. Hamley, I. W. The Physics of Block Copolymers; Oxford University Press: New York, 1998.
2. Bates, F. S.; Fredrickson, G. H. *Phys. Today* 1999, 52, 32.
3. Abetz, V.; Goldacker, T. *Macromol. Rapid Commun*. 2000, 21, 16.
4. Alexandridis, P.; Spontak, R. *J. Curr. Opin. Colloid Interface Sci.* 1999, 4, 130.
5. (5) Hanley, K. J.; Lodge, T. P. *J. Polym. Sci. B: Polym. Phys.* 1998, 36, 3101. Hanley, K. J.; Lodge, T. P.; Huang, C.-I. *Macromolecules* 2000, 33, 5918.
6. Lodge, T. P.; Pan, C.; Jin, X.; Liu, Z.; Zhao, J.; Maurer, W. W.; Bates, F. S. *J. Polym. Sci. B: Polym. Phys.* 1995, 33, 2289.
7. Hong, S.-U.; Laurer, J. H.; Zielinski, J. M.; Samseth, J.; Smith, S. D.; Duda, J. L.; Spontak, R. J. *Macromolecules* 1998, 31, 2174.
8. Alexandridis, P.; Olsson, U.; Lindman, B. *Langmuir* 1998, 14, 2627.
9. Laurer, J. H.; Khan, S. A.; Spontak, R. J.; Satkowski, M. M.; Grothaus, J. T.; Smith, S. D.; Lin, J. S. *Langmuir* 1999, 15, 7947.
10. Mischenko, N.; Reynders, K.; Koch, M. H. J.; Mortensen, K.; Pedersen, J. S.; Fontaine, F.; Graulus, R.; Reynaers, H. *Macromolecules* 1995, 28, 2054. Reynders, K.; Mischenko, N.; Mortensen, K.; Overbergh, N.; Reynaers, H. *Macromolecules* 1995, 28, 8699.
11. Raspaud, E.; Lairez, D.; Adam, M.; Carton, J.-P. *Macromolecules* 1996, 29, 1269.

12. Soenen, H.; Berghmans, H.; Winter, H. H.; Overbergh, N. *Polymer* 1997, 38, 5653. Soenen, H.; Liskova, A.; Reynders, K.; Berghmans, H.; Winter, H. H.; Overbergh, N. *Polymer* 1997, 38, 5661.

13. Hamley, I. W.; Pople, J. A.; Booth, C.; Yang, Y. W.; King, S. M. *Langmuir* 1998, 14, 3182. Hamley, I. W. *Curr. Opin. Colloid Interface Sci.* 2000, 5, 342. Daniel, C.; Hamley, I. W.; Mortensen, K. *Polymer* 2000, 41, 9239.

14. Durrschmidt, T.; Hoffmann, H. *Colloid Polym. Sci.* 2001, 279, 1005.

15. Vega, D. A.; Sebastian, J. M.; Loo, Y.-L.; Register, R. A. *J. Polym. Sci. B: Polym. Phys.* 2001, 39, 2183.

16. Laurer, J. H.; Mulling, J. F.; Khan, S. A.; Spontak, R. J.; Bukovnik, R. *J. Polym. Sci. B: Polym. Phys.* 1998, 36, 2379. Laurer, J. H.; Mulling, J. F.; Khan, S. A.; Spontak, R. J.; Lin, J. S.; Bukovnik, R. *J. Polym. Sci. B: Polym. Phys.* 1998, 36, 2513. 8266 Langmuir 2002, 18, 8266-8270

17. Watanabe, H.; Sato, T.; Osaki, K.; Yao, M.-L.; Yamagishi, A. *Macromolecules* 1997, 30, 5877. Watanabe, H.; Sato, T.; Osaki, K. *Macromolecules* 2000, 33, 2545.

18. Quintana, J. R.; Diaz, E.; Katime, I. *Langmuir* 1998, 14, 1586.

19. Jackson, N. R.; Wilder, E. A.; White, S. A.; Bukovnik, R.; Spontak, R. J. *J. Polym. Sci. B: Polym. Phys.* 1999, 37, 1863.

20. Theunissen, E.; Reynaers, H. L.; Mortensen, K. Unpublished results.

21. Spontak, R. J.; Wilder, E. A.; Smith, S. D. *Langmuir* 2001, 17, 2294.

22. Quintana, J. R.; Hernaez, E.; Katime, I. *Polymer* 2002, 43, 3217.

23. Halperin, A.; Zhulina, E. B. Europhys. Lett. 1991, 16, 337. Zhulina, E. B.; Halperin, A. *Macromolecules* 1992, 25, 5730.

24. King, M. R.; White, S. A.; Smith, S. D.; Spontak, R. J. *Langmuir* 1999,15, 7886.

25. Kavanagh, G. M.; Ross-Murphy, S. B. *Prog. Polym. Sci.* 1998, 23, 533.

26. van Maanen, G. J.; Seeley, S. L.; Stevens, J. E.; Bukovnik, R. R.; Spontak, R. J. Manuscript in preparation.

27. Balazs, A. C.; Lewandowski, S. *Macromolecules* 1990, 23, 839.

28. Kumacheva, E. Personal communication, 2002.

Chapter 4: Property Development in Nanocomposite Thermoplastic Elastomer Gels (NCTPEGs)

4.1 Abstract

Thermoplastic elastomer gels (TPEGs), molecular networks composed of a microphase-separated multiblock copolymer swollen to a large extent by a low-volatility midblock-selective solvent, are ubiquitous in a wide range of contemporary technologies, including home and office products, athletic equipment and telecommunications devices. In this work, we investigate the effect of several network-forming nanoscale modifiers — two different silica nanoparticles, 3 different nanoclays and a multiwalled carbon nanotube — on the property development of a TPEG prepared from a microphase-ordered poly(styrene-*b*-(ethylene-*co*-butylene)-*b*-styrene) (SEBS) triblock copolymer imbibed with an EB-compatible aliphatic mineral oil. Dynamic rheological measurements of the resultant nanocomposite TPEGs (NCTPEGs) confirm that addition of these modifiers tends to increase the linear viscoelastic threshold, the dynamic elastic modulus (G') and the flow onset temperature (where G' plummets) of the parent TPEG. Variable-temperature stress-relaxation studies indicate that these NCTPEGs undergo substantial relaxation irrespective of added modifier at temperatures above ~60°C. Complementary x-ray diffraction analysis reveals that the nanoclay particles used to generate three series of the NCTPEGs examined here are swollen with copolymer and/or solvent and are therefore intercalated.

4.1 Introduction

Block copolymers, macromolecules composed of two or more long, contiguous sequences of chemically-dissimilar repeat units, continue to remain a subject of intense research and technological interest due to their inherent ability to spontaneously assemble into a wide variety of nanostructures — spherical or cylindrical micelles, bicontinuous channels, co-alternating layers and complex combinations thereof — in the melt.[1-4] The formation of such nanostructures not only provides fundamental insight into the mechanism of molecular self-organization but also provides a platform by which to develop multifunctional materials for waveguides,[5] nanotemplates,[4-7] nanoporous media,[9,10] nanopattern transfer and permselective membranes.[9-12] This rich phase behavior likewise extends to block copolymers swollen in the presence of a neutral or block-selective liquid solvent.[15-17] A recent study suggests that this paradigm may be general, further extrapolating to compressible (i.e., supercritical) solvents. In this study, we focus on linear multiblock, more precisely ABA triblock, copolymers highly swollen in a low-volatility B-selective solvent. If the A blocks of the microphase-separated copolymer are glassy or semicrystalline and the B blocks are molten at application temperature and the B blocks generate an interconnected network by forming bridges between adjacent A microdomains,[19-21] the neat copolymer can be described as a thermoplastic elastomer (TPE).[22,23] Addition of a B-selective solvent at sufficiently high concentration ultimately causes the copolymer molecules to adopt a spherical micelle morphology to minimize repulsive contacts between the A units and the B-rich solvent matrix. If the micelles

remain molecularly interconnected, the swollen copolymer behaves as a physical gel and can therefore be termed a thermoplastic elastomer gel (TPEG).[22]

Numerous studies reported[28] over the past decade have sought to establish fundamental relationships between morphology and property development in TPEGs as explicit functions of copolymer molecular weight, copolymer composition, solution concentration, solvent quality and process (temperature and shear) history. One of the most highly investigated copolymer families explored in this vein consists of commercially available poly(styrene-*b*-(ethylene-*co*-butylene)-*b*-styrene) (SEBS) triblock copolymers, which are employed in a diverse range of contemporary technologies. An illustrative transmission electron microscopy (TEM) image of a TPEG composed of 10 wt% SEBS copolymer in 90 wt% (EB-selective) aliphatic mineral oil[22] is presented in Fig. 4.1 and verifies the micellar morphology anticipated from complementary small-angle scattering results. A shortcoming of TPEGs derived on the basis of the SEBS copolymer is an inherently low modulus and a relatively low maximum operating temperature (MOT) identified as the temperature at which the gel network no longer supports an applied load and the solution flows as the modulus decreases precipitously. Efforts designed to improve the properties and stability of styrenic TPEGs have modified (*i*) the micellar core through the incorporation of a homopolymer that mixes athermally or exothermically[20] (χ, the Flory-Huggins interaction parameter, is zero or negative, respectively) with the S blocks of the copolymer, (*ii*) the micellar corona via addition of chemically-identical diblock copolymer that alters chain packing and the propensity for midblocks to form bridges, and (*iii*) the midblock-rich solvent matrix through the addition of a semicrystalline homopolymer[22] that is compatible

with the S blocks. Note that, in all these previous endeavors, the TPEG modifier has been an organic species.

A successful alternative route by which to form stable physical gels in organic solvents and oligomers is through the incorporation of inorganic nanoscale objects such as fumed silica and nanoclays. These systems rely on specific surface interactions, such as hydrogen bonding, to form solid-like (gel) networks wherein the dynamic elastic modulus (G') is independent of oscillatory frequency (ω) and consistently greater than the dynamic viscous modulus (G").[22] As with the copolymer-forming networks described above, colloidal networks such as these are also sensitive to concentration, solvency, temperature and shear history. The purpose of this work is to marry these two gel formulation strategies and generate nanocomposite thermoplastic elastomer gels (NCTPEGs) consisting of both organic and inorganic interpenetrating networks. It is in this spirit that a broad range of inorganic nanoscale objects, including two different nanoparticles, three different nanoclays and a multiwalled nanotube, have been incorporated into the TPEG pictured in Fig. 4.1 to ascertain the effects of modifier concentration, surface chemistry and shape on mechanical property development in these reinforced hybrid NCTPEGs.

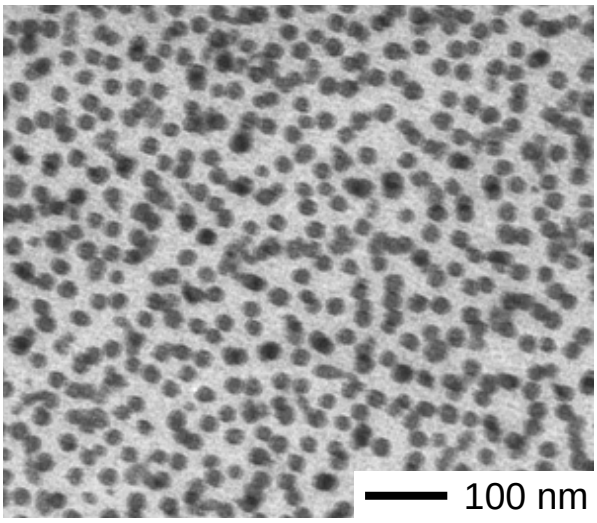

Figure 4.1: TEM image of a block copolymer gel composed of 10 wt% SEBS and 90wt% mineral oil.

This work serves to extend our previous analyses[20-22] of organically-modified TPEGs and the recent report of silica-reinforced TPEGs by Theunissen et al.[25] The results obtained here further add to the insight gleaned from ongoing experimental[26,27] and theoretical[28] studies of solvent-free block copolymer nanocomposites prepared by physical dispersion of nanoscale objects.

4.2 Experimental section

4.2.1. Materials

The SEBS triblock copolymer with a number-average molecular weight of 161,000 g/mol and 31 wt% S was manufactured by Kraton (Houston, TX) and used as-received. Methyl-terminated (hydrophobic) fumed silica (FS, 12 nm primary particle size) was obtained in powder form from Degussa Corp. (Aerosil® R974, Parsippany, NJ), whereas silanol-terminated (hydrophilic) colloidal silica (CS, 20 nm mean particle size) was supplied by Nissan Chemicals (Organosilicasol® MEK-ST-MS, Houston, TX) as a suspension (30% solids) in methyl ethyl ketone. Two montmorillonite clays organically modified[52] with methyl tallow bis-2-hydroxyethyl ammonium chloride (Cloisite 30B, abbreviated C30B) or dimethyl tallow 2-ethyl hexyl ammonium chloride (Cloiste 93A, abbreviated C93A) were provided by Southern Clay Products (Gonzales, TX), whereas a tetraalkyl ammonium hectorite (Bentone 38, denoted B38) was supplied by Elementis Specialties (Hightstown, NJ). Their densities were 1.98, 1.88 and 1.70 g/cm^3, respectively. A multiwalled carbon nanotube (NT) with a mean diameter of 80 nm and length of 5 μm was obtained from Sun Nanotech Co. (Nanchang, China). The mineral oil (MO) was Witco Hydrobrite 380 with a molecular weight of about 503 g/mol and a density of 0.87 g/cm^3 (Crompton Corp., Petrolia, PA). Reagent-grade ethanol, chloroform and propylene carbonate were purchased from Aldrich Chemicals (St. Louis, MO) and used without further purification.

4.2.2. Methods

Hybrid gels composed of 10 wt% SEBS copolymer, 1 wt% Irganox antioxidant, 0-10 wt% inorganic modifier and 79-89 wt% MO were prepared by high shear dispersion in a double-planetary mixer operated under vacuum for 1 h (30 min at 20 Hz and 30 min at 40 Hz) at 180°C. These process parameters were the same as those used in previous studies[20,22] to permit direct comparison and maintain reproducibility. To facilitate dispersion within the nonpolar MO, the B38 and NT modifiers were first immersed and agitated in propylene carbonate and chloroform, respectively, before they were added to their predesignated SEBS/MO mixtures. While chloroform pretreatment assisted in NT dispersion, field-emission scanning electron microscopy (FESEM) images such as the one displayed in Fig. 4.2 confirmed that the NT size distribution is broad. Upon cooling to ambient temperature, all the resultant hybrid gels were compression-molded for 10 min at 180°C to yield films measuring 1.5-2.0 mm in thickness. Variation in mixing or molding temperature yielded no discernible change in the measured properties. Circular specimens (25 mm in diameter) were stamped from the films and stored between sheets of wax paper under dark and cool conditions to avoid degradation prior to analysis.

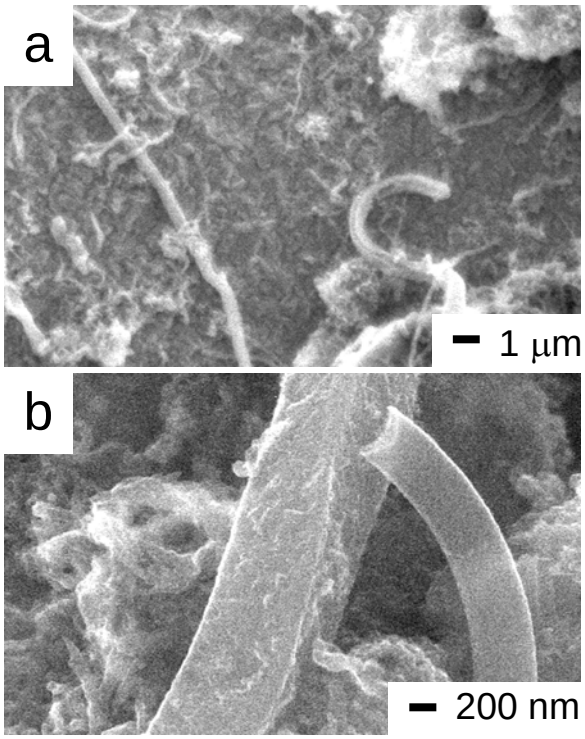

Figure 4.2: Field - emission scanning electron microscopy (FESEM) images of the multi walled carbon nanotubes

Dynamic shear measurements were conducted on two different instruments: an ATS RheoSystems Stresstech rheometer and a Rheometrics ARES rheometer. Shear stress analyses conducted at $\omega = 1$ rad/s identified the range of the linear viscoelastic (LVE) regime wherein G' and G" are independent of the applied stress (τ).[29] Frequency spectra confirmed that G' was independent of ω and consistently greater than G" (by at least an order of magnitude) at a stress within the LVE limit for each gel.[29] The thermal response of selected NCTPEGs was discerned by discretely ramping temperature and monitoring G' at each temperature after an equilibration period of 1 min. (Continuous-ramp tests yielded qualitatively similar results, but showed signs of thermal hysteresis and were not used for

that reason.) Variable-temperature stress-relaxation tests were conducted in the LVE regime by subjecting NCTPEGs at their highest concentration (10 wt% for CS, C93A, C30B and B38, but only 3 wt% for FS and NT) to 1% strain and recording the stress decay over the first 200 s. X-ray diffractometry (XRD) was performed on the pure nanoclays, as well as on NCTPEGs with 5 and 10 wt% nanoclay, with an Inel XRG 3000 diffractometer operated at 35 kV and 30 mA using monochromated Cu K_α radiation over the 2θ range 2-120° to discern the effect of SEBS and/or MO on the morphology of the platelets.

4.3 Results and discussion

4.3.1. Property enhancement at ambient temperature

The dependence of the dynamic elastic modulus (G') on stress (τ) for the unmodified SEBS/MO gel is provided in Fig. 4.3. The corresponding values of G" are equally well-behaved, but consistently more than an order of magnitude less than G', and are not included for these reasons. The data shown in Fig. 4.3 clearly demonstrate that the LVE limit extends to ~6 kPa, as estimated by the intersection of two tangents drawn through the data at high and low τ. This value of τ can be considered a dynamic yield stress (τ_y) since G' decreases abruptly with increasing τ (indicating collapse of the load-bearing network) beyond this value.[23]

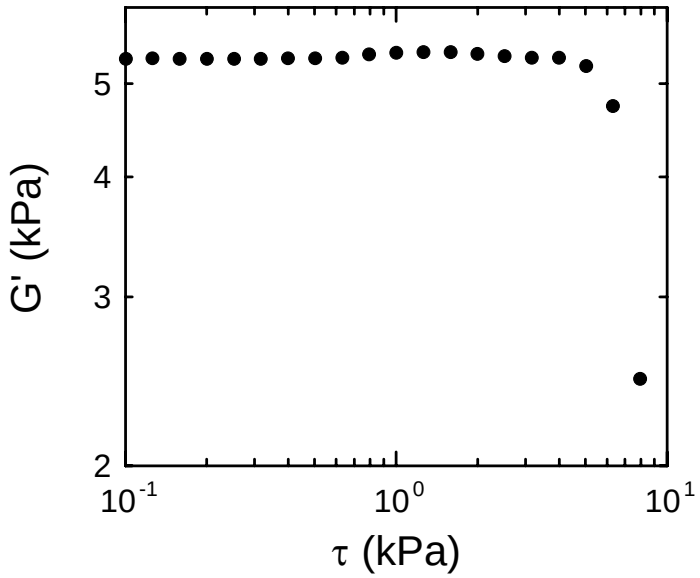

Figure 4.3: Dependence of the dynamic elastic modulus (G') on stress (τ) for the unmodified SEBS/MO gel.

Analogous G'(τ) signatures for NCTPEGs containing varying concentrations of the CS and FS nanoparticles are presented for comparison in Fig. 4.4. While an increase in modifier concentration is observed to promote a general increase in G', the presence of CS nanoparticles appears in Fig. 4.4(a) to have a deleterious effect on τ_y, which suggests that, at low concentrations, the CS nanoparticles interfere with the connectivity of the underlying copolymer network. A scenario that is consistent with this notion requires the CS nanoparticles to be so highly dispersed that individual nanoparticles physically obstruct the formation of bridges between neighboring micelles. It should be mentioned here that a high level of CS nanoparticle dispersion has been recently achieved[56] in a poly(methyl methacrylate) matrix. At higher concentrations, the CS nanoparticles are anticipated to

flocculate into large-scale aggregates and hinder to a lesser extent the bridging efficacy of individual copolymer molecules. No such reduction in τ_y is evident for FS in Fig. 4.4(b). This invariance in τ_y may reflect the preponderance of permanently fused aggregate structures commonly encountered with FS. One other unexpected feature of the data shown in Fig. 4.4(a) (not seen in Fig. 4.4(b)) is that at the highest concentration examined (10 wt% CS), G' decreases gradually with increasing τ, indicative of limited network alteration, prior to plummeting as the network ultimately collapses.

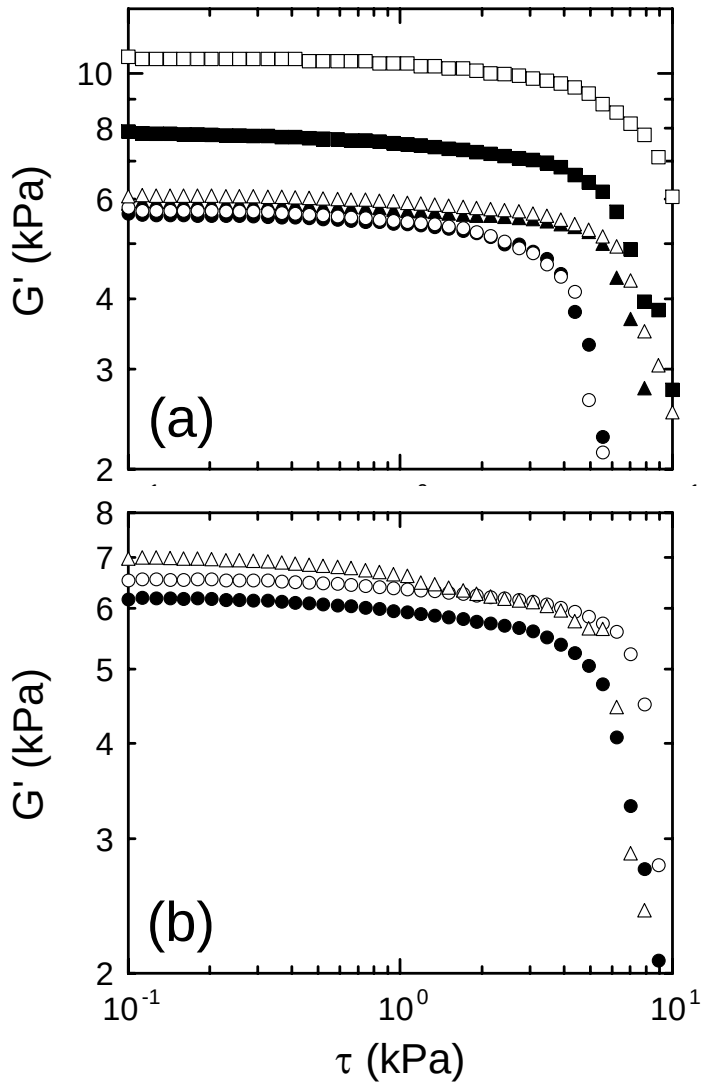

Figure 4.4: Influence of (a) CS and (b) FS on the dynamic mechanical properties of SEBS/MO gels. Symbols mean different concentrations: 0.5 wt% (filled circle), 1 wt% (unfilled circle), 2 wt% (filled triangle), 3 wt% (unfilled triangle), 5 wt% (filled square), 10 wt% (unfilled square)

Comparable G'(τ) responses acquired from the nanoclay- and NT-modified gels are provided in Figs. 4.5 and 4.6, respectively. In the case of the two organically-modified montmorillonites (C93A in Fig. 4.5(a) and C30B in Fig. 4.5(b)), an increase in nanoclay concentration is seen to promote a monotonic increase in G' in the LVE threshold and an initial increase in a discernible τ_y at low concentrations. At high concentrations, however, the stress-induced reduction in G' again becomes increasingly more gradual before decreasing precipitously. Similar behavior is observed for NCTPEGs prepared with the B38 hectorite nanoclay (*cf*. Fig. 4.5(c)) with the notable exception that the gradual reduction in G'(τ) occurs systematically with increasing nanoclay concentration. This apparent gradual reduction observed in Fig. 4.5 is contrary to a previous report by Walls et al.[24] of a Li-exchanged organoclay incorporated into poly(ethylene glycol) (PEG). In their study, G' is found to remain constant over the entire LVE regime and then fall sharply at τ_y. Note that such behavior is, in fact, characteristic of the TPEGs modified with NT.

Thus, we propose that, at high concentrations, the nanoclay-modified gels undergo some level of nanostructural rearrangement upon deformation prior to network collapse at τ_y. An implication of this conclusion is that the nanoclay platelets must be intercalated with either the SEBS copolymer or the MO, since neither a fully immiscible microcomposite nor a fully exfoliated nanocomposite would be expected to exhibit such rearrangement that would yield a discernible change in G'. This consideration will be further addressed in a later section.

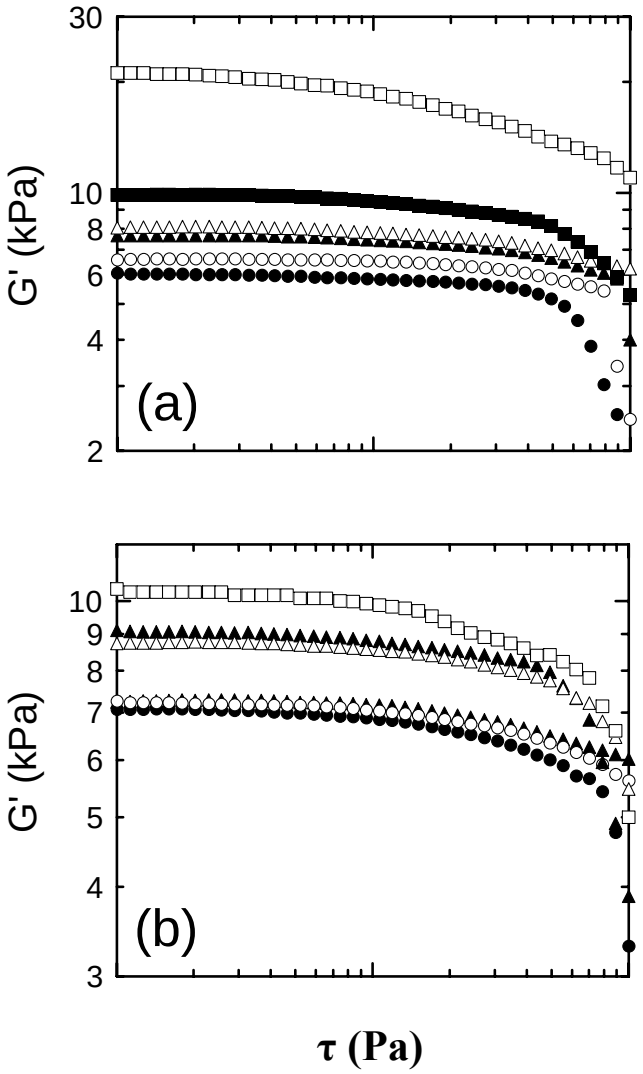

Figure 4.5: Influence of (a) C93A and (b) C30B on the dynamic mechanical properties of SEBS/MO gels. Symbols mean different concentrations: 0.5 wt% (filled circle), 1 wt% (unfilled circle), 2 wt% (filled triangle), 3 wt% (unfilled triangle), 5 wt% (filled square), 10 wt% (unfilled square)

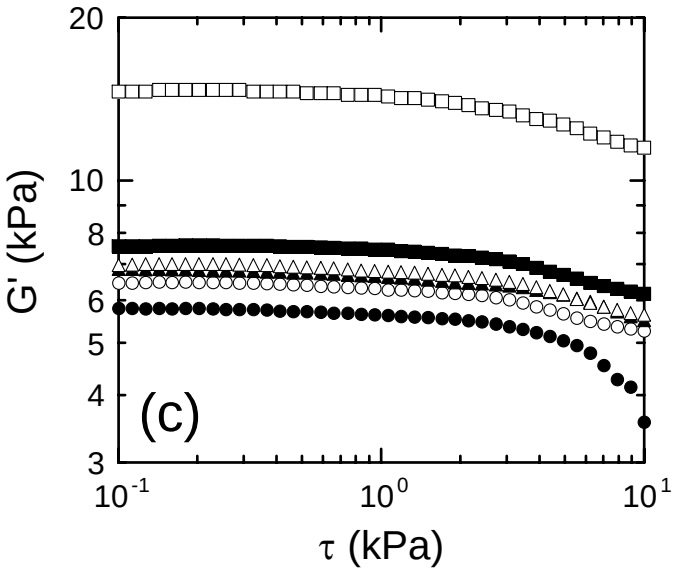

Figure 4.5: Influence of (c) B38 on the dynamic mechanical properties of SEBS/MO gels. Symbols mean different concentrations: 0.5 wt% (filled circle), 1 wt% (unfilled circle), 2 wt% (filled triangle), 3 wt% (unfilled triangle), 5 wt% (filled square), 10 wt% (unfilled square)

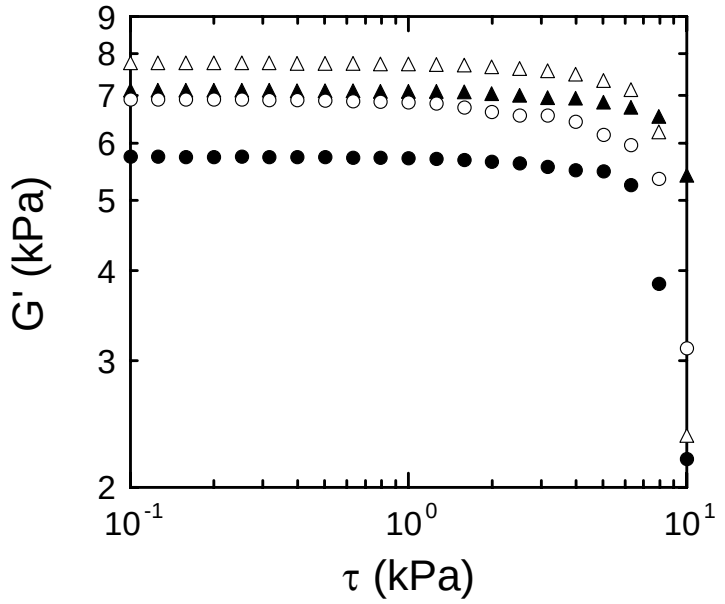

Figure 4.6: Influence of the NT on the dynamic mechanical properties of SEBS/MO gels. Symbols mean different concentrations: 0.5 wt% (filled circle), 1 wt% (unfilled circle), 2 wt% (filled triangle), 3 wt% (unfilled triangle).

Values of the plateau G' extracted from the data presented in Figs. 4.3-4.6 are displayed in Fig. 4.7 as a function of modifier concentration (C, in wt%) for the CS and FS nanoparticles (Fig. 4.7(a)), the C93A, C30B and B38 nanoclays (Fig. 4.7(b)) and the NT (Fig. 4.7(c)). Included for comparison in each part of Fig. 4.7 are data collected[22] from TPEGs possessing higher SEBS concentrations. If the 10 wt% SEBS TPEG is considered the reference material, then a TPEG with 15 wt% SEBS, for example, will contain 5 wt% SEBS additive. In most cases, addition of any of these inorganic modifiers at low concentrations (up to 3 wt%) yields G' values that are nearly coincident (within experimental uncertainty) with those of the neat TPEGs varying in SEBS content. Only the CS nanoparticle system (Fig. 4.7(a)) yield a markedly lower G' in this concentration range. At the highest concentrations explored here (5 and 10 wt%), the CS nanoparticle- and the C30B nanoclay-modified gels exhibit virtually identical values of G'. It is interesting that these two species possess hydrophilic surface groups that are capable of interparticle hydrogen-bonding in nonpolar media (such as MO). Measured values of G' collected from the C30B and B38 NCTPEGs (Fig. 4.7(b)) likewise show a plateau at intermediate C, beyond which G' from the B38-modified gels increases sharply.

The hydrophobic C93A nanoclay-modified gel is the only system wherein G'(C) follows that of the TPEGs varying in SEBS concentration up to 10 wt% modifier. Adition of the NT to the SEBS/oil gel (Fig. 4.7(c)) likewise promotes a modest increase in G' over its limited concentration range (dictated by dispersion problems encountered at higher concentrations). Values of G' previously reported for a TPEG modified with syndiotactic homopolystyrene (shS), which forms long, highly dispersed crystals within the EB-rich solvent matrix, are included for comparison in Fig. 4.7(c). In all cases other than the

NCTPEGs produced with the C93A nanoclay, however, G' values evaluated at high C are markedly lower than those of unmodified TPEGs when modifier concentration is expressed in terms of C.

If the mass densities of the inorganic species employed here are known, then the modifier concentrations can alternatively be expressed in terms of volume percent. The nanoclay densities provided in the Experimental Section are used, for instance, to translate 10 wt% to about 5 vol% according to $W_{mod}/[W_{mod} + W_{SEBS}(w_S\rho_{mod}/\rho_S+w_{EB}\rho_{mod}/\rho_{EB}) + W_{MO}\rho_{mod}/\rho_{MO} + W_{aox}\rho_{mod}/\rho_{aox}]x100\%$. Here, W_i and ρ_i (i = mod for *mod*ifier, SEBS, MO or aox for *a*ntio*x*idant) are the weight fraction and density of component i, respectively, and w_j (j = S or EB) is the weight fraction of block j in the SEBS copolymer. To estimate the density of the FS, we assume that the nanoparticles possess a spherical shape so that the density can be expressed[57] as 6/(SxD), where S denotes the BET surface area and D is the mean particle diameter. The values of S and D reported by the manufacturer yield a density of ~2.5 g/cm^3. Similarly, the density of the CS can be estimated from the CS/MEK suspension density if Amagat's law (volume additivity) is applicable. If the suspension density lies between 1.0 and 1.2 g/cm^3, the density of CS is calculated to be 2.3-2.7 g/cm^3, and so an average value of 2.5 g/cm^3 is adopted in the following section. Lastly, we assume that the NT possesses a density that is comparable to that of graphite, namely, ~2.2 g/cm^3. The densities of amorphous polystyrene, crystalline polystyrene and liquid poly(ethylene-*co*-butylene) at ambient temperature are taken as 1.05, 1.13 and 0.86 g/cm^3, respectively.

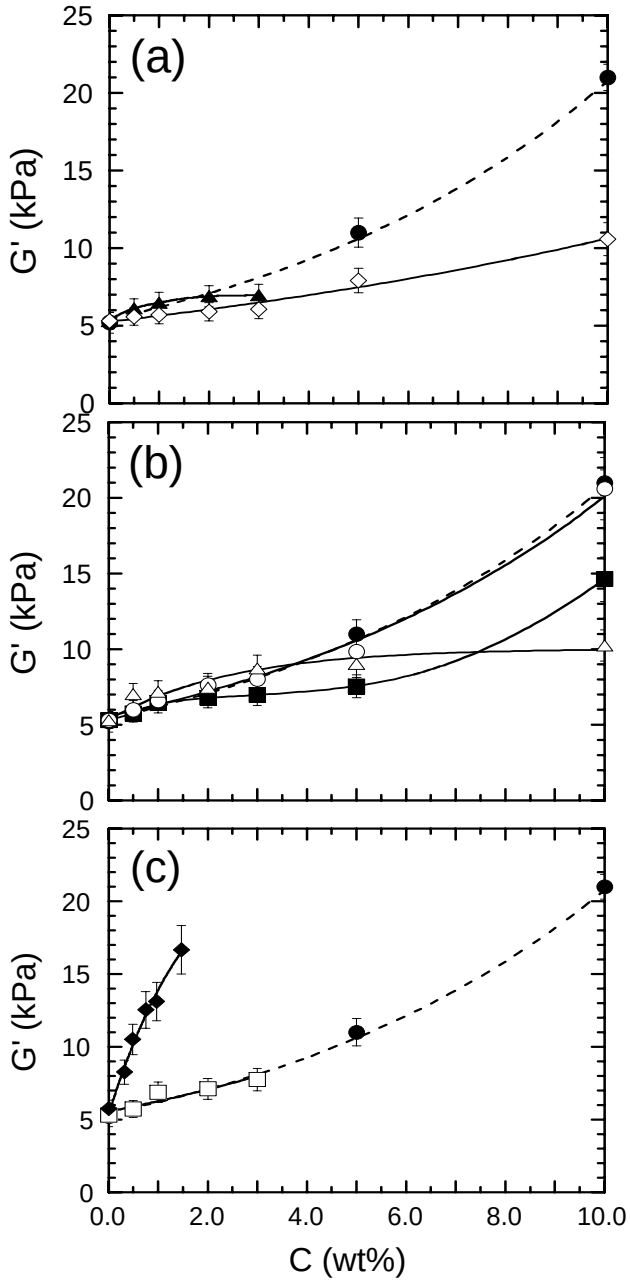

Figure 4.7: Values of the plateau G' as a function of modifier concentration. Symbols represent different modifiers: CS (unfilled diamond), FS (filled triangle), C93A (unfilled circle), C30B (filled square), B38 (unfilled triangle), NT (unfilled square), higher SEBS concentrations (filled circles), shS (filled diamond)

Figure 4.8 is a compilation of the G' values measured from all the NCTPEGs examined in this study, as well as the shS mentioned earlier,[22] presented as a function of modifier concentration (Φ, in vol%). In this format, addition of any of these modifiers is generally observed to promote an improvement in the mechanical properties of the NCTPEGs relative to unmodified TPEGs differing in SEBS content. The substantial improvement afforded by the C93A nanoclay in Fig. 4.8(a) most likely reflects its hydrophobic nature and ease of dispersion within the nonpolar MO matrix. In contrast, the slight improvement gained by the NT in Fig. 4.8(b) indicates that a high aspect ratio alone does not ensure property enhancement and supports our earlier conclusion[22] that the long shS crystals (filled diamond) selectively interact with the S blocks of the copolymer to strengthen the shS-modified TPEG. Such interaction certainly warrants further investigation.

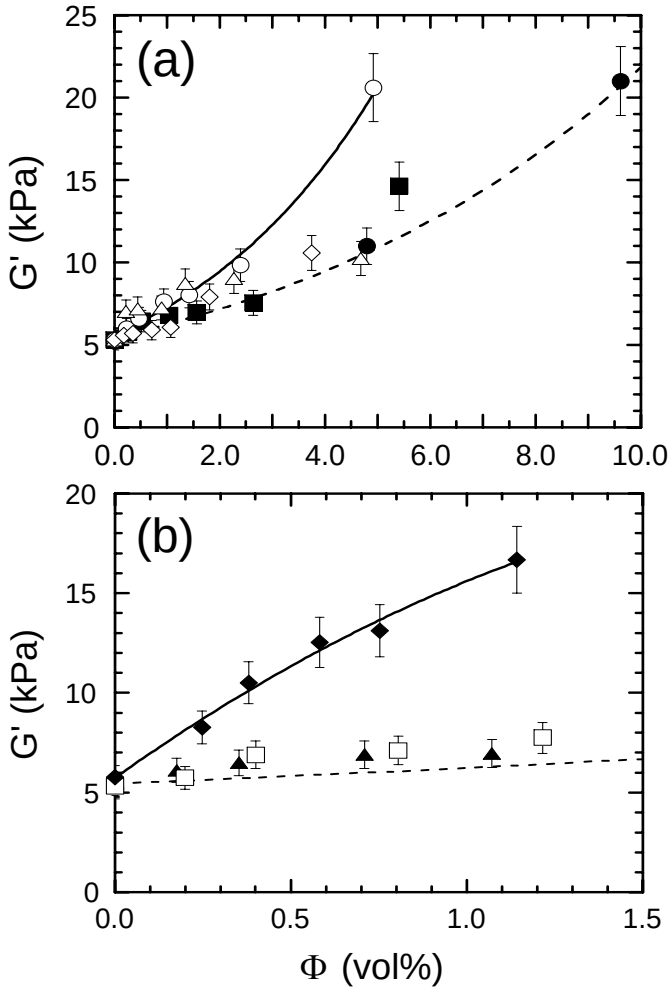

Figure 4.8: Compilation of the G' values measured from all the NCTPEGs examined in this study, as well as the shS mentioned in Chapter 3, presented as a function of modifier concentration (Φ, in vol%). Symbols represent different modifiers: CS (unfilled diamond), FS (filled triangle), C93A (unfilled circle), C30B (filled square), B38 (unfilled triangle), NT (unfilled square), higher SEBS concentrations (filled circles), shS (filled diamond)

4.3.2. Property enhancement at elevated temperatures

The variation in G' with temperature (T), normalized with respect to G' evaluated at 30°C, at a constant strain of 2% is presented in Fig. 4.9 for the parent TPEG and the two NCTPEGs having up to only 3 wt% modifier — FS (Fig. 4.9(a)) and NT (Fig. 4.9(b)). The signature of the unmodified SEBS/MO gel consists of four characteristic regions: (*i*) an initial plateau over which G' remains relatively constant or increases slightly with increasing temperature, (*ii*) an abrupt reduction in G' attributed to a lattice disordering transition in the vicinity of 95°C, (*iii*) a second plateau in G' at about 130°C and (*iv*) a precipitous decrease in G' signifying the collapse of the copolymer network at *ca*. 150°C. Similar results with the exception of the second plateau have been previously reported[22] for the same unmodified TPEG. Existence of this new feature reflects the persistence of a residual, load-bearing nanostructure that either remains intact or develops upon increasing temperature. Mortensen and co-workers[18] have demonstrated that similar TPEGs exhibit a high-temperature body-centered cubic phase that possesses an unusually high degree of nanostructural order. This plateau is not, however, attributed to subtle differences in specimen preparation, since it remains after systematic variation of the mixing and pressing temperatures and times used to prepare the gel.

One of the most important characteristics of TPEGs is the maximum operating temperature (MOT), defined here as the temperature corresponding to region (iv), *i.e*., the onset of liquid-like behavior. The values of G' acquired from the NCTPEGs produced with FS (Fig. 4.9(a)) and NT (Fig. 4.9(b)) show negligibly little change (< 8°C) in the MOT.

Clearly, these inorganic modifiers have very little impact on the mechanical properties of the SEBS/MO TPEGs under investigation over the concentration range examined.

Values of G' measured from the remaining NCTPEGs (containing CS (open square), C93A (filled diamond), C30B (open triangle) or B38 (open cicrcle)) are displayed as a function of temperature in Fig. 4.10 for two different modifier concentrations — 5 and 10 wt%. While the modifiers increase the magnitude of G' at a concentration of 5 wt% (Fig. 4.10(a)), none extend the MOT by more than ~9°C. Similar results are evident for most of the modifiers at 10 wt% (Fig. 4.10(b)). The one exception is the NCTPEG composed of 10 wt% C93A nanoclay, which undergoes a sharp reduction in G' at about 162°C and then develops a third G' plateau in the vicinity of 180°C. This new plateau extends the MOT to beyond 200°C and strongly suggests the existence of secondary (nanoclay) network that remains surprisingly stable at relatively high temperatures. Increasing the MOT of any NCTPEG prepared here to *ca*. 200°C constitutes a sensible limit, since the SEBS copolymer may start to degrade and the MO will evaporate upon exposure to higher temperatures. Thus, the hydrophobic C93A nanoclay serves two important purposes in the design of NCTPEGs derived from SEBS/MO TPEGs: by forming a secondary network at sufficiently high concentrations, this modifier simultaneously increases the gel strength (expressed in terms of G') and the MOT. While we recognize that it may be possible to achieve comparable results with the other inorganic modifiers examined here at higher concentrations, the promising performance of the C93A nanoclay in this study certainly merits continued investigation.

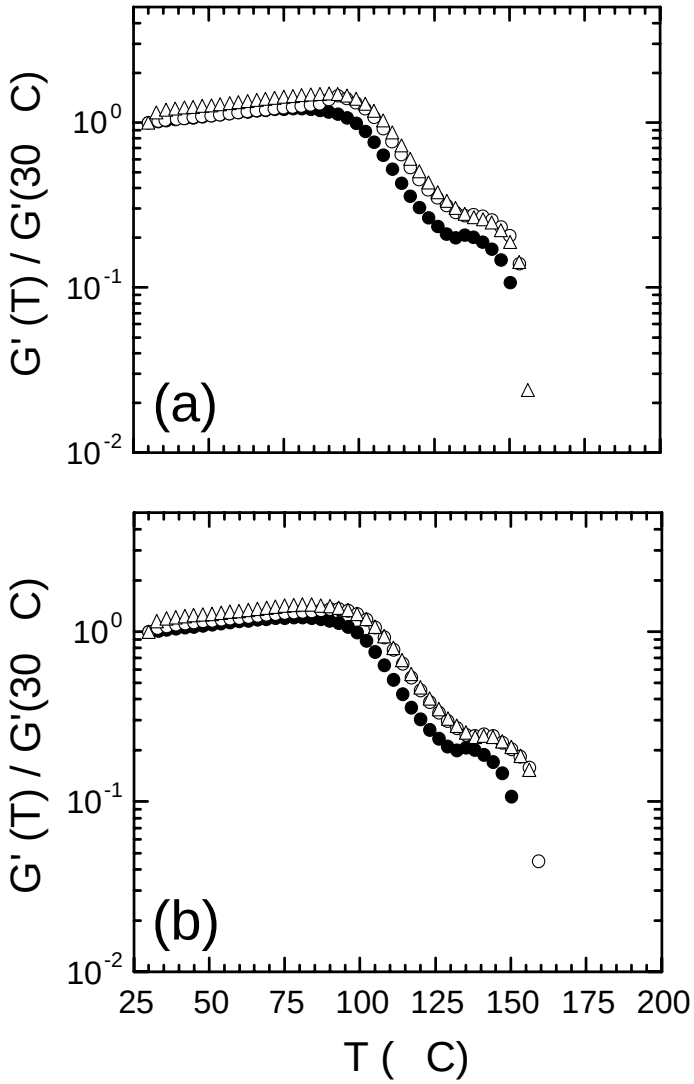

Figure 4.9: The variation in G' with temperature (T), is presented for the parent TPEG and the two NCTPEGs having up to only 3 wt% modifier — (a) FS and (b) NT.

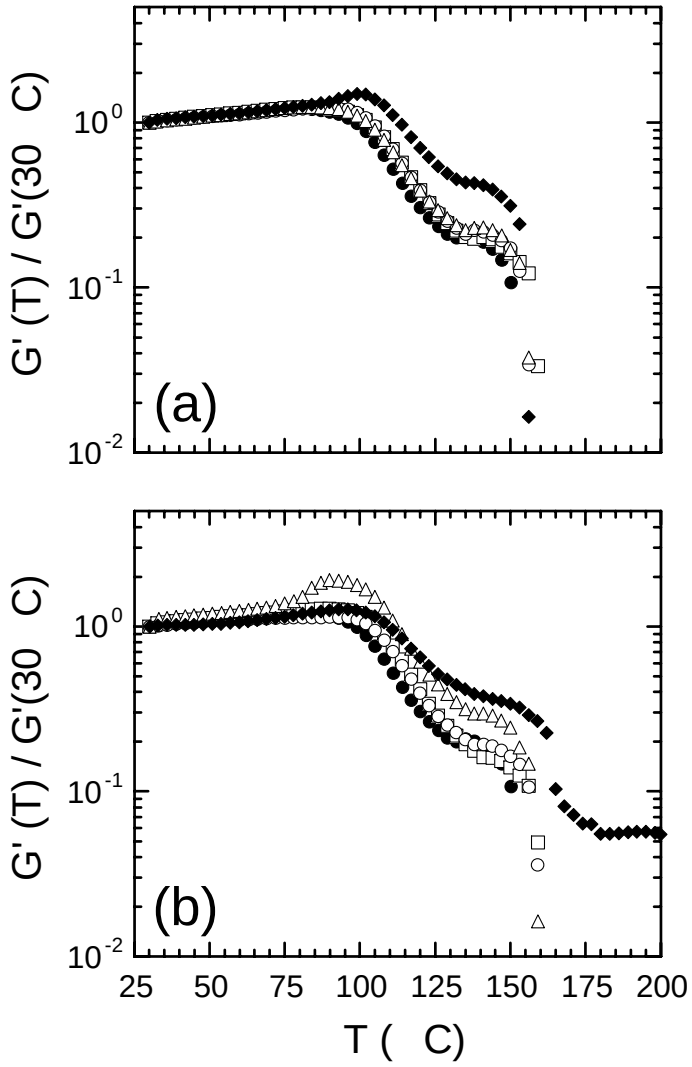

Figure 4.10: The variation in G' with temperature (T), is presented for the parent TPEG and the two NCTPEGs having two concentrations: (a) 5 wt% and (b) 10 wt%. Symbols represent different modifiers: C93A (filled diamond), C30B (unfilled triangle), B38 (unfilled circle), CS (unfilled square), neat copolymer (filled circle)

4.3.3. Modifier effect on NCTPEG stress relaxation

Since the incorporation of inorganic nanoscale objects into a polymer matrix can have a profound effect on the properties of the polymer, we have elected to examine the temperature-dependent stress-relaxation behavior of NCTPEGs containing 10 wt% modifier. Representative examples of relaxation curves collected from different specimens of the NCTPEG modified with 3 wt% NT at several temperatures (in 10°C increments) up to 70°C are provided in Fig. 4.11.

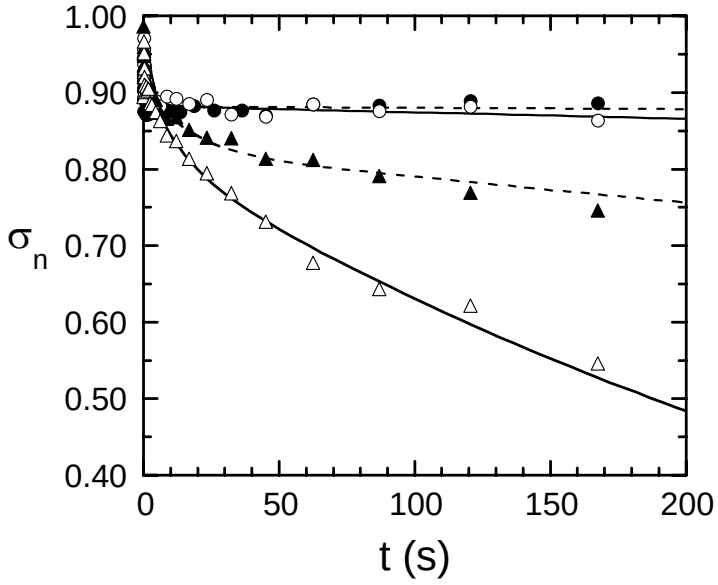

Figure 4.11: Relaxation curves collected from the NCTPEG modified with 3 wt% NT at several temperatures. Symbols mean different temperatures: 30°C (filled circle), 40°C (unfilled circle), 60°C (filled triangle) and 70°C (unfilled triangle)

A common feature of these data, expressed in terms of the stress normalized with respect to the initial stress, is that they consistently exhibit comparable degrees of relaxation up to 50°C. Progressively more extensive relaxation occurs at 60 and 70°C, as the materials approach the glass transition temperature (T_g) of the S blocks comprising the network-stabilizing micelles and soften. These stress-relaxation curves can be analyzed in terms of the general Zener model,[29] which relates the normalized stress (τ_n) to characteristic time scales associated with distinct relaxation processes by

$$\tau_n = \Sigma_i A_i \exp (- t / \lambda_i) \quad (1)$$

Here, A_i is the *i*th pre-exponential coefficient, t is time and λ_i denotes the *i*th relaxation time. Fitting Eq. 1 to relaxation data such as those provided in Fig. 12 requires three terms (k = 3) to achieve the satisfactory regressions included in the figure. This analysis generally indicates the existence of three relaxation processes possessing different characteristic time ranges (in s): (*i*) λ_1 = 0.03 – 0.2, (*ii*) λ_2 = 1 – 60 and (*iii*) λ_3 = 400 – 20000. (The values of A_i are neither physically meaningful nor insightful, and are not included here for these reasons.) The first two relaxation times do not correlate with respect to temperature, whereas the temperature dependence of λ_3 can be satisfactorily described by an Arrhenius expression of the form

$$\lambda_3 = \lambda_0 \exp (E_a / RT) \quad (2)$$

where λ_0 is a constant, R is the universal gas constant and E_a is the corresponding activation energy of the long-time relaxation process. An example of λ_3 presented as a function of reciprocal temperature for the NCTPEG containing 10 wt% C30B nanoclay is displayed for illustrative purposes in Fig. 4.12. Values of E_a obtained from linear

regression of Eq. 2 to the values of λ_3 extracted from Eq. 1 range from 46 kJ/mol for the C93A-modified NCTPEG to 78 kJ/mol for the NT-modified NCTPEG. It is interesting that the C93A nanoclay, the modifier capable of promoting the greatest difference in the rheological properties of the TPEG, possesses the lowest E_a of the entire series. The E_a values deduced for the CS-, FS- and B38-modified gels lie between 48 and 52 kJ/mol, whereas the C30B system possesses a marginally higher E_a (66 kJ/mol).

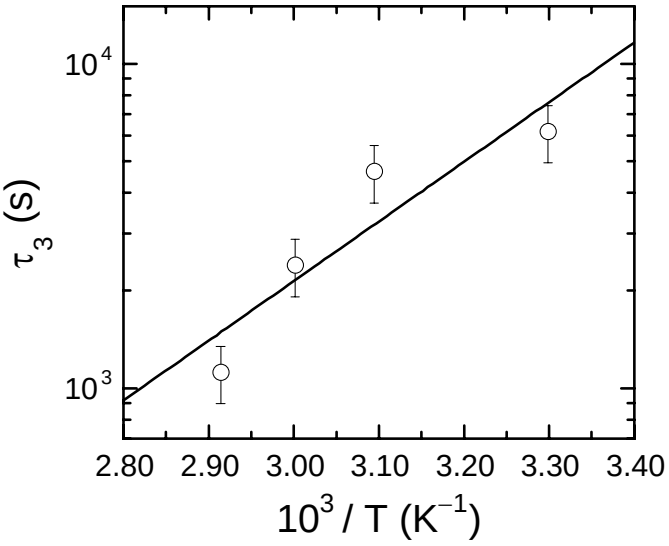

Figure 4.12: An example of λ_3 (third relaxation time) as a function of reciprocal temperature for the NCTPEG containing 10 wt% C30B nanoclay.

4.3.4. Morphological analysis of nanoclay-modified TPEGs

X-Ray Diffraction (XRD) was used in order to characterize the morphology of the different NCTPEGs. Figure 4.13 gives XRD patterns for: (a) C93A, (b) C30B and (c) B38 and six composites. All these different types of nanoclays are considered layered silicates.

Different types of interactions can take place between polymeric systems and organic layered silicates (OLS). For inmiscible mixtures of polymers and OLS, the basal reflection of the clay does not change upon blending with the polymer. Now, when intercalation takes place, there is a finite layer expansion that results into a larger gallery height; obtaining a new basal reflection. At the same time, intercalated systems can be either ordered or disordered. In the case of ordered intercalated systems, a new basal (and well defined) reflection peak can be seen. At the same time higher order peaks can also be seen. On the other hand, disordered intercalated systems exhibit peak broadening and intensity loss due to a decrease in the degree of coherent layer stacking. In the case of exfoliated systems, due to extensive layer separation (beyond the resolution of Bragg-Brentano geometry), is not possible to observe a new basal reflection peak. This leads to intensity loss and disappearance of the unintercalated basal reflection.[30]

All three NCTPEGs modified with nanoclays exhibit intercalation, as it can be seen in Figure 4.13 (the small shift on the basal reflection peak to the left indicates an increase in the gallery height). The system filled with C30B exhibits a more disordered structure than the other cases, as indicated by a basal reflection peak broadening. Also, the interlayer gallery spacing in the NCTPEGs is independent of the silicate loading .

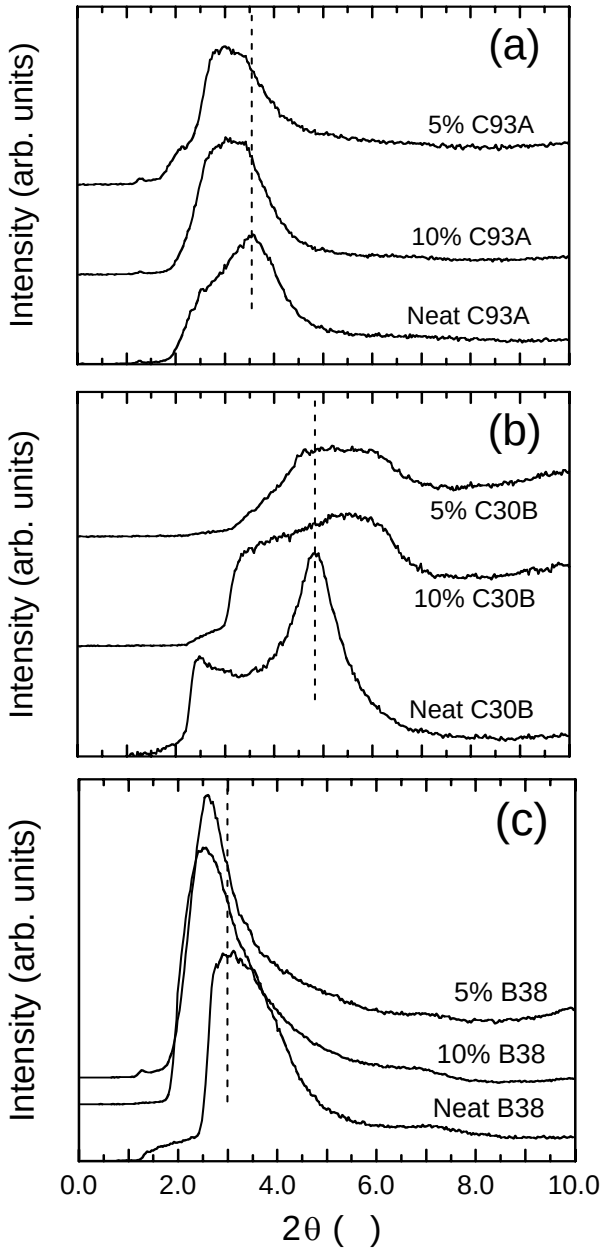

Figure 4.13: X-Ray Diffraction Patterns for different nanoclays and NCTPEGs

4.4 Conclusions

Addition of different types of inorganic nanofillers to a micellar SEBS/oil gel at constant oil content serves to reinforce the gel, as evidenced by a pronounced increase in G'. This increase reflects the formation of a secondary network that reinforces the primary network formed by the gel. These nanofillers differ in size and shape, seeing how their aspect ratio affects the mechanical properties; an increase or a decrease, in the value of G', can be seen as the aspect ratio changes. Temperature sweeps indicate an increase in the MOT of all the different NCTPEGs, being the system filled with C93A the one that exhibits the best enhancement in properties. From a morphological point of view, there is enough evidence to justify the formation of an intercalated structure in all cases. Also, the concentration of the layered silicates does not affect the basal reflection of the nanoclays. The results presented here demonstrate that the properties of ABA block copolymer solutions may be controllably and substantially modified through the addition of inert fillers.

4.5 Acknowledgments

We thank SINTEF for the carbon nanotubes and partial financial support, and Professors S.A. Khan and C.R. Daubert (North Carolina State University) for generous access to their rheometers.

4.6 References

1. I.W. Hamley. The physics of block copolymers. Oxford Science Publications. New York, NY (1998).
2. F.S. Bates; G.H. Fredrickson. *Phys. Today* 52, 32 (1999)
3. N. Hadjichristidis; S. Pispas; G. Floudas. Block copolymers : synthetic strategies, physical properties, and applications. Wiley. Hoboken, N.J. (2003)
4. I.W. Hamley. Developments in block copolymer science and technology. Wiley. Hoboken, N.J. (2004)
5. P.D. Yang; A.H. Rizvi; B. Messer; B.F. Chmelka; G.M. Whitesides; G.D. Stucky. *Adv. Mater.* 6, 427 (2001)
6. M. Templin; A. Franck; A. Du Chesne; H. Leist; Y. Zhang; R. Ulrich; V. Schädler; U. Wiesner. *Science* 278, 1795 (1997)
7. P.F.W. Simon.; R. Ulrich; H.W. Spiess; U. Wiesner. *Chem. Mater.* 10, 3464 (2001)
8. V. I. Bondar, B. D. Freeman, I. Pinnau. *J. Polym. Sci. Part B* 17, 2463 (1999)
9. J. H. Kim; E. J. Moon; C. K. Kim. *J. Membr. Sci.* Volume 216, Issues 1-2, Page 107 (2003)
10. N.P. Patel; R.J. Spontak. *Macromolecules* 4, 1394 (2004)
11. J.H. Laurer; S.A. Khan; R.J. Spontak. *Langmuir* 15, 7947 (1999)
12. P. Alexandridis; R.J. Spontak. *Curr. Opin. Colloid In* 2, 130 (1999)
13. L. Kane; D.A. Norman; S. A. White; M. W. Matsen; M. M. Satkowski; S. D. Smith; R. J. Spontak. *Macromol. Rapid Commun.* 22, 281 (2001)
14. R.J. Spontak; N.P. Patel. *Curr Opin Coll Interface Sci* 5, 334 (2000)

15. J.H. Laurer; J. F. Mulling; S. A. Khan; R. J. Spontak; R. Bukovnik. *J. Polym. Sci. Part B* 13, 2379 (1998)

16. Mischenko, N.; Reynders, K.; Koch, M. H. J.; Mortensen, K.; Pedersen, J. S.; Fontaine, F.; Graulus, R.; Reynaers, H. *Macromolecules* 28, 2054 (1995).

17. Reynders, K.; Mischenko, N.; Mortensen, K.; Overbergh, N.; Reynaers, H. *Macromolecules* 28, 8699 (1995)

18. K. Mortensen; E. Theunissen; R. Kleppinger; K. Almdal; H. Reynaers. *Macromolecules* 35, 7773 (2002)

19. J.H. Laurer; J.F. Mulling; S.A. Khan; R.J. Spontak; J.S. Lin; R. Bukovnik. *J. Polym. Sci. Part B* 14, 2513 (1998)

20. N.R. Jackson; E.A. Wilder; S.A. White; R. Nukovnik; R.J. Spontak. *J Polym Sci Part B* 37, 1863 (1999)

21. R.J. Spontak; E.A. Wilder; S.D. Smith. *Langmuir* 8, 2294 (2001)

22. T.A. Walker; J.J. Semler; D.N. Leonard; G.J. van Maanen; R.R. Bukovnik; R.J. Spontak. *Langmuir* 18, 8266 (2002).

23. S.A. Khan; S.R. Raghavan. *J. Rheol.* (39) 6, 1311 (1995)

24. H.J. Walls; M.W. Riley; R.R. Singhal; R.J. Spontak; P.S. Fedkiw; S.A. Khan. *Adv. Funct. Mater* 13, No. 9, 1 (2003)

25. E. Theunissen; N. Overbergh; H. Reynaers; S. Antoun; R. Jerome; K. Mortense. *Polymer* 45, 1857 (2004).

26. R. Krishnamoorti; R.A. Vaia; E.P. Giannelis. *Chem. Mater.* 8, 1728 (1996).

27. R. B. Thompson; V.V. Ginzburg; M. W. Matsen; A. C. Balazs**.** *Science* 292, 2469 (2001)

28. A.J. Schultz; C.K. Hall; J. Genzer. *J Chem Phys* 22, 10329 (2002)

29. C.W. Macosko. Rheology Principles, Measurements and Applications, Wiley-VCH (1994)

30. R.A. Vaia; E.P. Giannelis. *Macromolecules* 30, 7990 (1997).

Chapter 5: Conclusions

Recently, Polymer Layered Silicate (PLS) nanocomposites became commercially available, and were applied to the automotive industry;[1] also, biodegradable polymer based nanocomposites appear to have a very bright future for a wide range of applications as high performance biodegradable materials; this indicates and gives an idea on how important this type of materials are and how they can be found in daily activities. The principal objective of this study has been to study how, by adding different types of inert fillers and an A compatible semi-crystalline homopolymer (shS) to a thermoplastic elastomer gel composed of a SEBS copolymer and mineral oil, the morphology and bulk properties of the system change.

Dynamic Rheological experiments performed on all samples indicate a reinforcement of the gel, as evidenced by a pronounced increase in the dynamic elastic modulus (G'). In the case of the clays, montmorillonite organoclays and hectorite, is suggested that a mesoscopic structure of randomly oriented silicate layer tactoids form a three-dimensional percolated network structure, even at low silicate loadings, reinforcing the network formed by the physical gel. As expected, as you increase the filler content (in all the cases) the G' value increases. The TPGE filled with the alkyl terminated layered silicate (C93A) gives the highest G' value of all the fillers, G'≈21 kPa, at a concentration of 10 wt.%. In the case of the silica, the gels are significantly reinforced by the presence of silica particles in the rubbery matrix, but not as effective as in the case of the layered silicates; i.e. in the case of colloidal silica, at 10 wt.%, the system has a G'≈10kPa. The case of the TPEG filled with an A-compatible semi-crystalline homopolymer (shS) shows

that the shS is far more effective in improving gel stiffness than inert fillers, which could be attributed to the interaction between the nanoscale shS objects and the Styrene (A-block) rich micelles (as seen in TEM images). The drawback of this additive is that the viscosity of the melt increases significantly, as was shown by surface measurements.[2] Another point observed by rheological studies, was an increase in the Maximum Operating Temperature (MOT) of the system for all the different fillers; G' remains constant to a lattice disordering temperature and then plummets at MOT. The positive influence on the transition temperature from a viscoelastic rubber to a plastic fluid is one of the most important features induced by the presence of fillers in the triblock copolymer gel, an observation, which can be helpful to widen the applicability of these types of low molar mass triblock copolymer gels into a higher temperature regime. It can be said that all the samples with a filler concentration of 10 wt.%, exhibit an increase in the MOT of about 70°C; just to put in contrast, the TPEG with no fillers has a MOT ≈ 90°C while filled TPGEs have a MOT ≈ 160°C. The TPGE filled with the alkyl terminated layered silicate (C93A) exhibits an interesting feature and that is that even after the MOT the G' value remains constant, developing a plateau. This indicates that structure is held together by the mesoscopic structure of randomly oriented silicate layers that forms a percolated network.[3]

These improved properties are generally attained at lower silicate content compared to that of conventionally filled systems. For these reasons, Polymer Layered Silicates nanocomposites are far lighter in weight than conventional composites, and make them competitive with other materials for specific applications.

Finally, the fact that PLS nanocomposites show concurrent improvement in various material properties at very low filler content, together with the ease of preparation through simple processes, opens a new dimension for these types of materials.

5.1 References

1. J.M. Garces; D.J. Moll; J. Bicerano; R. Fibiger; D.G. McLeod. Adv Mater (12) 23, 1835 (2000)
2. E. Kumacheva. Personal communication (2002)
3. J. Ren; A.S. Silva; R. Krishnamoorti. Macromolecules 33, 3739 (2000)

Chapter 6: Future Work

Vaia et al.[1] suggested the development of Lewis base interactions between Polystyrene derivative polymers and Organically Modified Layered Silicates (OMLS), where the benzene ring (in the Polystyrene derivative) would act as a donator and the layered silicate would act as an acceptor. IR could be a useful tool to determine if these interactions take place, by comparing the spectrum of the pure SEBS/Mineral Oil with the spectrum of the SEBS/OMLS/Mineral Oil.

It is known that due to the high degree of inter-tube bonding possible per carbon nanotube, it is virtually impossible for them to organize by only the means that kinetic thermal energy contributes.[2] Ultrasound has also been used as a way to dispersed untreated nanotubes, but a considerable amount of damage can be caused on the surface; defects as bending, buckling and dislocations can be seen on the nanotubes.[3] Mason[4] has proved that damage on nanotubes is solvent dependent, less damage has been observed in water and ethanol, but there is always the possibility of damage and the possibility of insolubility with the rest of the components in a system. Surface treatment should be considered in order to improve dispersion; Shaffer et al.[2], by using aqueous acid, oxidize the surface of the nanotubes introducing oxygen-containing functional groups. Their results showed the formation of a well dispersed-stable colloid in water. Another method could be the use of commercially available dispersants composed by a block copolymer and a solvent. Zhao et al.[5] have proved effective-stable multi-walled carbon nanotubes dispersions in ethanol by using one of these dispersants mentioned above.

6.1 References

1. Vaia R.A.; Giannelis E.P. Macromolecules 30, 7990 (1997)

2. M.S.P. Shaffer; X. Fan; A.H. Windle. Carbon 11, 1603 (1998)

3. P.J.F. Harris; M.L.H. Green; S.C. Tsang. J Chem Soc Faraday Trans 89, 1189 (1993)

4. T.J. Mason. Practical Sonochemistry Ellis Horwood Ltd. Chichester, UK (1991)

5. L. Zhao; L. Gao. Colloids and Surfaces A: Physicochem Eng Aspects 224, 127 (2003).